PAPER

Check for updates

Unveiling the dye adsorption capability of *Moringa oleifera* functionalized hybrid porous MOF–GO composites: *in vitro* and *in silico* ecotoxicity assessment *via* antibacterial and molecular docking studies†

Anil Kumar K.,[a] Arpit Bisoi,[a] Yeshwanth M.,[b] Shobham,[c] Mohan Jujaru,[a] Jitendra Panwar 🆔*[c] and Suresh Gupta 🆔*[a]

The present study demonstrated the synthesis of sustainable and eco-friendly composites composed of Fe & Al metal–organic frameworks (Fe-MOF and Al-MOF) and their graphene oxide composites (AlGC and FeGC). Post-synthetic surface functionalization of developed composites was done with *Moringa oleifera* leaves powder extract. The synthesized MOFs and composites were characterized using standard techniques. The ability of synthesized MOFs and composites to remove methyl orange (MO) and methylene blue (MB) dyes from wastewater was evaluated. Based on the higher dye removal ability, detailed dye adsorption studies were performed with functionalized composites (AlGC and FeGC). Taguchi optimization design was utilized to optimize the four testing factors, *viz.* contact time, initial dye concentration, composite dosage, and temperature, along with five levels for each factor to achieve the highest capacity for dye adsorption. The composites exhibited outstanding equilibrium adsorption capacities for MO (AlGC: 577 ± 37 and FeGC: 631 ± 42 mg g^{-1}) and MB (AlGC: 336 ± 13 and FeGC: 387 ± 7 mg g^{-1}) dyes, which are found to be the highest among the reported composites so far. Applying isotherms, kinetics, and thermodynamic models confirmed the spontaneous, endothermic reactions for the physisorption of both dyes. The regeneration studies showed more than ~65% dye removal efficiency of both the composites up to three adsorption–desorption cycles, which confirms their reusability at the industrial scale. The environmental toxicity of developed composites was analyzed by antibacterial studies against selected ecologically important soil bacteria as well as by molecular docking studies against protein targets of selected microorganisms.

Water impact

Adsorption is favoured for wastewater treatment due to its efficacy and versatility. MOFs are highly promising adsorbents with adjustable properties. However, challenges like cost and limited industrial use hinder their application. This study develops MOF–GO composites to enhance pollutant removal, promoting sustainable water treatment. Molecular docking and antimicrobial assays assess their environmental impact and efficacy, contributing to wastewater treatment advancements.

1. Introduction

Water is considered a vital resource on the planet, and the demand for it has increased due to the increase in population and rapid growth of industries. Recently, the worldwide wastewater generation has been estimated as 359.4 × 109 m^3 y^{-1}, of which only 52% (188.1 × 109 m^3 y^{-1}) was treated.[1] Unfortunately, this means that a substantial portion of wastewater remains untreated and poses environmental challenges. In general, industries such as textile, paper, leather, plastic, rubber, cosmetics, and food

[a] Department of Chemical Engineering, Birla Institute of Technology and Science, Pilani 333 031, India. E-mail: sureshg@pilani.bits-pilani.ac.in
[b] Department of Bioengineering, University of Pennsylvania, Pennsylvania 19104, USA
[c] Department of Biological Sciences, Birla Institute of Technology and Science, Pilani 333 031, India. E-mail: jpanwar@ pilani.bits-pilani.ac.in

† Electronic supplementary information (ESI) available. See DOI: https://doi.org/10.1039/d4ew00185k

1938 | *Environ. Sci.: Water Res. Technol.*, 2024, **10**, 1938–1963

This journal is © The Royal Society of Chemistry 2024

are mainly responsible for wastewater generation, of which dyes emanating from the textile industries drastically contaminate the water. Approximately 100 000 distinct compounds are used as dyes, and a substantial amount of dyes and pigments are utilized during the dyeing process. A yearly average of 12% of utilized synthetic dyes and ~27% of raw dyes are discharged *via* effluents into various water bodies, contributing to water pollution.[2] Methyl orange (MO) and methylene blue (MB) dyes are frequently utilized in textile and other industries. MO is categorized as an anionic dye within the azo dye group and contains a potentially hazardous azo (–N≡N–) group in its chemical structure.[3] Meanwhile, MB is a cationic dye extensively used in the textile industry. Both these dyes are reported to be toxic in water due to their complex structures, making their removal challenging as they are non-biodegradable and accumulate in environmental compartments.[4–6]

Various methods, including physical, chemical, physicochemical, and biochemical processes, have been investigated to remove these dyes.[4,7] Among physical methods, adsorption is the most preferred method for dye removal due to its simplicity, high efficiency, low energy requirement, reusability of the adsorbent, and ease of scaling up.[8] In recent years, various adsorption materials have been employed to treat industrial wastewater, including zeolites, clay, graphene, activated carbon, carbon nanotubes, polymeric resins, *etc.*[9] Among these, activated carbon stands out as a popular choice due to its exceptional porosity, strong interaction capabilities, chemical inertness, and non-toxic nature.[10] However, most of its pores have diameters less than 2 nm, which limits the capturing of bulk dye molecules on the inner surfaces, thereby reducing the proper utilization of its vast surface areas. Moreover, the commercially available activated carbons are costly and non-renewable.[11] Considering these drawbacks, there is an emerging need to synthesize materials with suitable pore sizes and large surface areas to remove dyes from wastewater.

In recent years, metal–organic frameworks (MOFs) have emerged as promising materials for removing dye contaminants from wastewater.[12,13] Compared to other porous adsorbents, MOFs offer several advantages, such as ultra-low density, well-defined ordered structures, large specific surface areas, ease of synthesis, and good thermal stability, which makes them suitable for the adsorption and removal of dyes from industrial wastewater.[14] Furthermore, their high stability in water, expansive surface area, and precise pore size make MOFs particularly effective in adsorbing and removing organic pollutants.[15] However, using expensive organic ligands such as terephthalic acid (TPA) and amino-terephthalic acid (NH₂–TPA) makes the synthesis process costly. In order to synthesize cost-effective MOFs, organic ligands can be derived from packing waste materials such as polyethylene terephthalate (PET), which mainly contains TPA and ethylene glycol (EG). Hydrolysis is a commonly used depolymerization method to recover TPA from PET waste, which is simple, cost-effective, and can significantly reduce the overall MOF synthesis cost.[16,17]

Among various MOFs, aluminum (Al) and iron (Fe)-based MOFs have gained significant attention due to their excellent thermal and adsorptive properties, and they have also been considered environmentally friendly.[18,19] However, the use of Al- and Fe-based MOFs is limited only to specific applications due to their instability in aqueous and other solvent media.[18,19] Compounding graphene oxide (GO) to Al- and Fe-based MOFs *via* an *in situ* synthesis procedure can overcome the structural instability of these MOFs in the aqueous medium. GO has recently attracted much interest due to its oxygen-containing functional groups, such as –OH, –COOH, and –CO, which provide a high negative charge density to GO and make it a superior material for water remediation applications.[20] Combining Al- and Fe-based MOFs with GO can overcome their instability problem in aqueous media. Moreover, their synergistic properties can enhance their dye adsorption capacity.

Enhancing the surface chemistry and morphology of composites by functionalization can further enhance their dye adsorption capability.[21–23] Various parts of the drumstick tree (*Moringa oleifera*), such as roots, stems, leaves, and husks, are a rich source of diverse compounds, including alkaloids, phenolics, carbohydrates, tannins, flavonoids, glycosides, phenols, proteins, and terpenoids.[24–27] These compounds can be extracted and utilized as functional groups on the surface of non-bonded metal and oxygen sites on the composite surfaces.[28] Applying these functionalized adsorbents holds great promise in the selective removal of specific dyes present in wastewater, making them effective adsorbents for improving water quality.

In general, the process of dye adsorption depends on various parameters, including equilibrium time, adsorbent dosage, solution temperature, adsorbate concentration, and pH, which necessitates the need for optimization of all the factors simultaneously using appropriate experimental design.[28] The choice of experimental design method depends on factors like system complexity, number of factors, precision, and resources. Taguchi's design offers efficient simultaneous optimization of all the parameters and their applicability to design industrial-scale processes.[28,29] Compared to other experiment design methods, such as central composite design (CCD) and response surface methodology (RSM), which require more experimental trials, the Taguchi design method is highly proficient in swiftly screening various parameters.[28,30,31]

Since the synthesis, utilization, and disposal of different MOFs and their composites will ultimately be discharged into the soil environment, they pose a potential threat to beneficial soil microorganisms.[14] Very limited reports have assessed the environmental toxicity of MOF-based composite materials toward soil microorganisms due to the intricate nature of the composite structures.[32–34] Hence, it is important to assess the toxicity of synthesized MOFs.

Considering the aforementioned facts, the present work aimed to synthesize Al- and Fe-MOF–GO composites following an environmentally sustainable method. It involves the

This journal is © The Royal Society of Chemistry 2024

Environ. Sci.: Water Res. Technol., 2024, **10**, 1938–1963 | **1939**

utilization of discarded PET bottles, aluminum foil waste, and ferric chloride hexahydrate (FeCl$_3$·6H$_2$O) as the source of organic ligands (TPA), Al, and Fe, respectively. The synthesizing MOFs were subsequently combined with GO and further surface functionalized by integrating functional groups derived from *Moringa* leaves powder. The developed composites were tested for their MO and MB dye removal efficiency from wastewater following the Taguchi optimization method. The intricate parametric batch adsorption experiments were carried out to estimate the kinetic, equilibrium, and thermodynamic parameters. Recycling studies were performed to check the composites' reusability. Given the possibility of the composites' release into the soil environment, antimicrobial assays and molecular docking studies were performed to study the toxicity of synthesized composites against selected soil microorganisms.

2. Materials and methods

2.1. Materials

The waste mineral water bottles (PET bottles) and aluminum foil were collected from the students' mess of BITS, Pilani, Rajasthan, India. The collected PET bottles and foil were sterilized by cleaning them with 70% ethanol. After cleaning, they were dried and cut into small pieces about 2 mm in size. These cut pieces were then stored for later use.

Analytical grade (AR) reagents with purity levels greater than 99% were employed throughout the study. The pre-processed 2 mm-sized PET particles, sodium hydroxide (NaOH; Merck, India), aluminium foil waste, ferric chloride hexahydrate (FeCl$_3$·6H$_2$O; Molychem, India), N,N-dimethyl formamide anhydrous (DMF) (C$_3$H$_7$NO; Spectrochem, India), 69–72% nitric acid (HNO$_3$; Molychem, India), and 35–37% hydrochloric acid (HCl; Molychem, India) were used for the synthesis of Al and Fe based MOFs.

A graphite flake, median 7–10 microns, 99% purity (Alfa Aesar, India), and *Moringa* powder (MP), >95% purity were utilized to GO synthesis and extraction of phytochemicals for post-synthetic functionalization of developed composites, respectively.

A synthetic aqueous dye solution of 1000 mg L^{-1} concentration for MO and MB (Merck, India) in Milli-Q water (Merck KGaA, Germany) was used for dye adsorption experiments.

Agar powder, Luria broth, and 10 mcg per disc tetracycline discs were procured from HiMedia, India. Meanwhile, pure isolates of bacterial strains, namely *Bacillus subtilis* MTCC 121 (Gram-positive bacterium) and *Escherichia coli* MTCC 1302 (Gram-negative bacterium), were procured from the Microbial Type Culture Collection and Gene Bank (MTCC), Chandigarh, India.

2.2. Synthesis of adsorbents

2.2.1. Phytochemical extract from MP. To extract phytochemicals, 40 g of MP were dispersed in a 4:6 v/v mixture of ethanol and water (400 mL) and subjected to reflux conditions at 80 °C for 4 h. The resulting mixture was cooled and filtered through Whatman no. 44 filter paper. The water from the obtained filtrate was evaporated under reduced pressure to produce a dense liquid extract, which was kept at 4 °C in a refrigerator for future use.

2.2.2. Isolation of TPA from PET bottles. Isolation of TPA using the alkaline hydrolysis method was described elsewhere.[35] Briefly, a sample of 5 g of small-sized PET pieces was added to 60 mL of 1 M NaOH solution. This mixture was then transferred to a Teflon-lined hydrothermal reactor with a capacity of 100 mL. The reactor was placed in an oven at a temperature of 150 °C for 4 h. After the reaction, the obtained solution was filtered to remove unreacted PET particles. The filtrate was then treated with 1 M HCl to precipitate TPA. The precipitated TPA was centrifuged at 7000 rpm for 7 min, followed by multiple washes with double distilled water to remove any by-products and excess acid. Finally, the TPA was dried under vacuum at 80 °C for 2 h and stored for future experiments.

2.2.3. Synthesis of GO. Hummer's method was used to synthesize GO with minor modifications.[36] Initially, a mixture of NaNO$_3$ (2.5 g) and graphite powder (5 g) was pulverized. The resulting mixture was added to an acidic solution composed of 108 mL H$_2$SO$_4$ (98%) and 12 mL H$_3$PO$_4$ solution in a 500 mL Erlenmeyer flask. Then, the flask was kept in an ice bath filled with a mixture of salt and ice, and the mixture was continuously stirred for 10 min on a magnetic stirrer. Subsequently, 15 g of KMnO$_4$ was gradually added to the solution while maintaining the temperature below 5 °C to prevent a sudden rise due to the exothermic reaction and stirred for 2 h. Afterward, the flask was removed from the ice bath and stirred for 60 min at 40 °C in a hot water bath. Then, 50 mL of distilled water was added to the mixture and stirred for an hour at 90 °C. The mixture was further diluted using distilled water to make a 400 mL suspension. After this, 15 mL of 30% H$_2$O$_2$ was added, which converted the solution into a bright yellow color. The solution was incubated at room temperature for 12 h. After incubation, the suspension was centrifuged at 8000 rpm for 7 min, and the obtained sediment was subjected to washing using a 5% HCl solution, followed by two additional washes with distilled water. The obtained GO was dried in a hot air oven at 60 °C for 24 h and converted into a fine powder using a mortar and pestle.

2.2.4. Preparation of the composite. 1 g of aluminium foil was dissolved in 20 mL of 6 M HCl. To this, 20 mL of concentrated HNO$_3$ was added, followed by heating to form an aluminium nitrate solution. Then, the solution was filtered to remove impurities and kept in a desiccator to form crystals of Al(NO$_3$)$_3$. The obtained crystals were purified by recrystallization using 20 wt% deionized water to get Al(NO$_3$)$_3$·9H$_2$O pure crystals. Al(NO$_3$)$_3$·9H$_2$O crystals were stored in an air-tight container as the metal precursor salt for the Al-based MOF synthesis.

MP extract was used to functionalize the developed MOF–GO composites. Fig. 1 illustrates schematically the key stages involved in synthesizing MOF–GO-based composites. The M-MOF (M: Al, Fe)/GO composite was synthesized by adding 0.78 g of Al(NO$_3$)$_3$·9H$_2$O (2.1 mmol)/0.675 g of FeCl$_3$·6H$_2$O
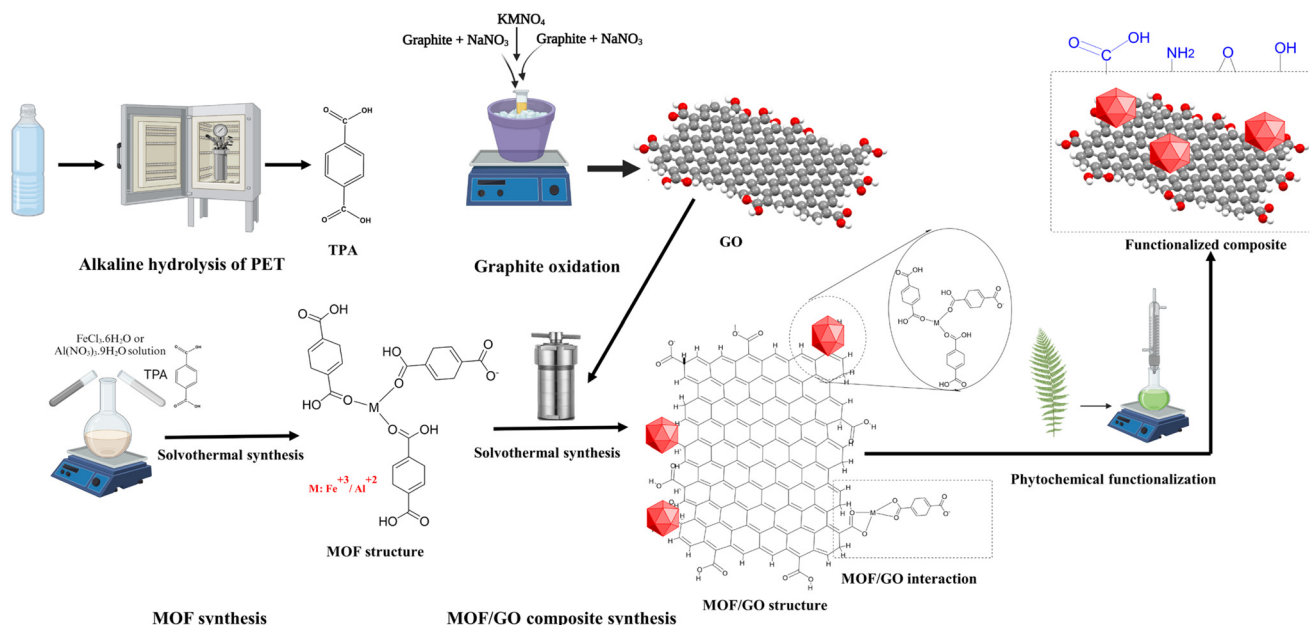
Fig. 1 Synthesis of the phytochemically functionalized GO/MOF composite.

(0.245 mmol) as a metal precursor and 0.206/0.518 g of TPA to a beaker containing 30/15 mL of DMF. Further, 39.4/135 mg of GO (5 wt%) was added to this mixture, and the resulting suspension was sonicated for 10 min and transferred into a Teflon-lined 100 mL hydrothermal reactor maintained at 130/110 °C for 72/20 h. The resulting solid particles were washed twice with DMF to remove unreacted TPA and then twice washed with ethanol and distilled water. The obtained particles were dried at 65 °C for 12 h, then pulverized to form fine particles of the Al-MOF–GO (AlG) and Fe-MOF–GO (FeG) composites. The prepared composite was added with 40 mL ethanol in a 250 mL Erlenmeyer flask for its surface functionalization. 3 mL of viscous MP extract was slowly added to this solution, and the resulting mixture was continuously agitated at a temperature of 70 °C for 24 hours. Later, the functionalized composite was separated by centrifugation and washed thrice with ethanol. The collected composite particles were vacuum-dried at 110 °C for 12 h. The obtained functionalized composites were denoted as AlGC and FeGC.

The pure Al-MOF, Fe-MOF, and unfunctionalized composites (AlG and FeG) were also kept to compare the difference in dye removal performance with functionalized composites (AlGC and FeGC).

2.2.5. Characterization. The functional groups, surface characteristics, elemental composition, and crystalline phases of GO, Al-MOF, Fe-MOF, AlGC, and FeGC were examined through standard analytical methods *viz.* field emission scanning electron microscopy (FE-SEM, ApreoLoVac, FEI), energy-dispersive X-ray spectroscopy (EDS, X-Max 80, Oxford Instruments), X-ray diffraction (XRD) using a RIGAKU Miniflex diffractometer, and Fourier transform infrared spectroscopy (FTIR, Frontier Spectrum 100 Series, USA, Perkin Elmer).[28,37,38]

Furthermore, the surface area, pore size, and pore distribution of the synthesized composites (AlGC & FeGC) were determined using N_2 gas adsorption isotherms through Brunauer–Emmett–Teller (BET) analysis at 77.35 K for 20.15 h and 7.2 h for Al-MOF and Fe-MOF based composites, respectively. Using a mortar pestle, the composites were ground, and any gases that had been adsorbing on their surfaces and pores were removed by degassing the mixture for two hours at 200 °C. The surface characteristics were determined using a BET analyzer (Autosorb-iQ TPX, Anton Paar), and thermal stability analysis of the synthesized composites was performed using a thermo gravimetric analyzer (TGA) (TG-4000, PerkinElmer) in a nitrogen atmosphere at a heating rate of 10 °C min^{-1} from 20–800 °C.[35,39] X-ray photoelectron spectroscopy (XPS, K-Alpha, Thermo Fisher Scientific Pvt. Ltd. UK) analysis was performed using a monochromatic Al Kα X-ray source operating at 1486.6 eV.

A pH meter (CyberScan pH 1100, Eutech Instruments) was used to determine the solution pH. The point of zero charge (pH_{ZPC}) for the synthesized composite was determined using the pH drift method. The detailed parameters used for analytical instruments and the sample preparation procedures were given in previous studies.[37,38]

A UV-vis spectrophotometer (Evolution 201, Thermo Scientific, USA) was utilized to measure the absorbance of the dyes, enabling quantification of MO and MB concentrations at wavelengths of 463.90 nm and 664.55 nm, respectively.[28]

2.3. Adsorption experiments

2.3.1. Performance evaluation of synthesized MOFs and composites. Prior to detailed parametric dye removal studies,

This journal is © The Royal Society of Chemistry 2024

Environ. Sci.: Water Res. Technol., 2024, **10**, 1938–1963 | **1941**

the performance of the synthesized MOFs and composites toward MO and MB dye adsorption was evaluated. Experiments were performed by adding 20 mg of the Al-MOF, Fe-MOF, AlG, FeG, AlGC, and FeGC separately to each flask containing 20 mL of 300 mg L^{-1} synthetic aqueous dye (MO and MB) solution. The flasks were placed in an incubator at a temperature of 25 °C with constant shaking at 150 rpm for an hour. Afterward, the flasks were removed, and the solution was centrifuged to separate the added adsorbents. The obtained samples were appropriately diluted to fall within the detection range, and the MO and MB concentrations were assessed by a UV-vis spectrophotometer. The percentage of MO and MB removal and the equilibrium loading were then determined using the equation outlined in the literature.[28]

2.3.2. Solution pH effect on adsorption of cationic and anionic dyes. The developed composites were studied to examine the influence of solution pH on removing both anionic (MO) and cationic (MB) dyes before examining various parameters influencing dye removal. The solution pH was singled out as a crucial factor due to its significant impact on dye adsorption, altering the composite's surface properties under acidic and basic conditions. Hence, it was vital to ascertain the optimal pH value for the batch experimental studies before performing the comprehensive parametric analysis.

For the adsorption experiment, 20 mL of respective dye solution (300 mg L^{-1}) were taken in 100 mL conical flasks. 0.2 M NaOH or 0.2 M HCl was used to adjust the initial solution pH, ranging from 2 to 12. Each flask was added with 20 mg of AlGC/FeGC (selected based on performance evaluation studies) and then incubated at 25 °C with a shaking speed of 150 rpm for 6 h. After that, the obtained solution was subjected to centrifugation to separate the composites from the solution. The obtained samples were appropriately diluted for analysis using a UV-vis spectrophotometer.

2.3.3. Taguchi optimization. The study aimed to evaluate the effectiveness of synthesized composites (AlGC and FeGC) in removing MO and MB dyes from aqueous solutions. Four input variables, *viz.* initial dye concentration (C_0, mg L^{-1}), composite dosage (m, mg), contact time (t, min), and operating temperature (T, °C), were analyzed during the optimization process. The levels of each factor are outlined in Table 1, and an L25 orthogonal array method was used to perform 25 sets of experiments based on the selected levels and factors (Table 1).

Table 1 Process input factors and their levels

S. No.	Factor A (t, min)	Factor B (m, mg)	Factor C (C_0, mg L^{-1})	Factor D (T, °C)
1	10	10	100	20
2	30	15	200	25
3	60	20	300	30
4	120	25	400	35
5	180	30	500	40

Taguchi optimization experiments were carried out by taking a fixed amount of composite in 100 mL conical flasks containing 20 mL of dye solution at the optimal pH condition (determined from the effect of pH studies). The input factors for each experimental run were maintained in the flasks as per the details given in Table S1,† and the flasks were kept for incubation. The flasks were taken out once the incubation process was finished, and the solution was subjected to centrifugation for 7 min at 7000 rpm. The supernatant was collected and diluted to fit within the UV-vis spectrophotometer's detection range. To ensure accuracy, each experiment was conducted in triplicate under identical conditions. Finally, analysis of variance (ANOVA) was used to validate the optimization results and identify the most critical factors impacting the adsorption process. The employed validation methodology was consistent with prior literature studies,[28,40] and a detailed analysis approach was utilized to ensure the accuracy and reliability of the model validation.

The final step of Taguchi optimization involves conducting confirmation experiments to examine the model's accuracy. Once the optimum factors have been selected, the response against those factors can be evaluated. The signal-to-noise (S/N) ratio (η_{opt}) utilizing optimum levels of the design parameters is calculated using the empirical formulas provided in eqn (1). Using the estimated η_{opt}, the predicted response (R_{opt}) can be calculated using eqn (2).[30,41]

$$\eta_{opt} = \eta_m + \sum_{i=1}^{q} (\bar{\eta}_i - \eta_m) \tag{1}$$

where η_m represents the S/N ratio's total mean, ($\bar{\eta}_i$) represents the S/N ratio's mean at the optimum level, and q is the number of the process factors that considerably affect the performance characteristic.

$$\left(\frac{S}{N}\right)_{HB} = -10 \log\left[\frac{1}{n}\sum_{i=1}^{n}\frac{1}{y_i^2}\right] \tag{2}$$

where 'n' is the number of tests repeated under the same conditions for a specific design factor, and 'y_i' represents the individual's adsorption capacity at the 'ith' experiment.

Adsorption experiments were conducted to evaluate the predicted response for the estimated optimum factors. The experimentally achieved adsorption capacity (q_{exp}, mg g^{-1}) was compared with the predicted adsorption capacity (q_{pred}, mg g^{-1}).

2.3.4. Parametric batch studies. To determine isotherm, kinetic, and thermodynamic parameters, a comprehensive study was conducted by performing batch adsorption experiments for MO and MB dyes (refer to Table 2) to assess the impact of t (min), C_0 (mg L^{-1}), T (°C), and m (mg). Each experiment involved 20 mL of synthetic dye solution in a 100 mL Erlenmeyer flask, with continuous agitation at 150 rpm. Later, the composite loaded in the solution was separated *via* centrifugation, and the collected filtrate was diluted appropriately for dye concentration analysis using a UV-vis spectrophotometer. The experimental results were then fitted with various models, including

1942 | *Environ. Sci.: Water Res. Technol.*, 2024, **10**, 1938–1963

This journal is © The Royal Society of Chemistry 2024

Table 2 The range of process parameter values used in batch studies

Parameters	t (min)	C_0 (mg L^{-1})	T (°C)	m (g L^{-1})
t	0–300	500	25	1
C_0	120	50–1300	25	1
T	120	500	15–40	1
m	120	500	25	0.5–2

Langmuir, Freundlich, Dubinin–Radushkevich (D–R), and Temkin for isotherms, pseudo-first & second order, and Elovich for kinetics, and van 't Hoff for thermodynamics. This approach provided valuable insights into the dye and composite interaction mechanisms.[37,38,42]

2.4. Competitive adsorption studies

Mixed dye solution (MO & MB) was exposed to 1 g L^{-1} of AlGC and FeGC to study the competitive adsorption performance of these dyes. Each dye concentration was kept at 250 mg L^{-1} to keep the total loading of dye similar to Taguchi's optimum conditions (500 mg L^{-1}). The experimental flasks were incubated at 25 °C and 150 rpm for 3 h. After incubation, the samples were centrifuged at 7000 rpm for 5 min to separate the dye-loaded composite. The obtained supernatant was diluted to achieve the detection range and analyzed using a UV-vis spectrophotometer for the final dye concentration.

2.5. Regeneration studies

The ability to reuse spent composites is crucial, as many prepared composites go unused due to the difficulty of removing the dyes from the composites. Disposing of spent composites to the environment may adversely impact the environment. Hence, removing the adsorbed dye from the spent composite and reusing it to minimize the disposal problems is important. For this, dye-saturated 100 mg composite and 25 mL of 0.01 M HCl and ethanol mixture (1 : 9 v/v) (optimized based on preliminary experiments) were added to a 100 mL conical flask. The flask was then agitated at 25 °C for 2 h. Further, the composite was separated from the solution by centrifugation, which was further oven-dried for 12 h at 60 °C before being reused in subsequent adsorption–desorption experiments. A total of 5 adsorption–desorption cycles were performed.

2.6. Environmental toxicity studies

The synthesized composites' toxicity was investigated by assessing the antimicrobial activity and molecular docking studies against specific ecologically significant microorganisms, considering that their production, utilization, and eventual disposal may result in environmental release. The composite can be exposed to representative bacterial, fungal, and algal strains under controlled conditions. The growth inhibition, cell viability, and reproductive potential may be thoroughly examined to determine the potential impact on environmental microbial communities.[28] Molecular docking

experiments are helpful in comprehending the composite's interactions with soil microbial biomolecules. Simulating binding interactions at the molecular level makes it easier to predict how MOF-based composite materials might affect important biomolecules required by environmental bacteria.[37,43,44] The combined findings of antibacterial and molecular docking studies would offer valuable insight into the ecological toxicity of the composite.

2.6.1. _In vitro_ studies. The glycerol stock was utilized to revive _E. coli_ and _B. subtilis_ cultures, which were allowed to grow in Luria broth for two generations. The standard microbial cell count assay[45] was accomplished using Luria agar plates with 1.5% agar and a pH of 7.0 ± 0.2.

Bacterial cultures ranging from 10^7 to 10^8 colony-forming units (CFU) per mL were exposed individually to the synthesized composites (FeGC and AlGC) at a concentration of 1 mg mL^{-1}, a dose determined efficiently for these composites. This exposure was carried out for 12 h at 37 °C. A 100 μL sample was taken from each treated bacterial culture and spread onto separate Luria agar plates. These plates were then incubated for an additional 12 h at 37 °C to evaluate the effect of the composites. Subsequently, bacterial growth was monitored using a colony counter, and the obtained values were quantified as CFU mL^{-1}.

The Kirby–Bauer disc diffusion susceptibility assay was employed to evaluate the antibacterial activity of the synthesized composites. For this, 100 μL of fresh bacterial cultures with a concentration of 10^8 CFU mL^{-1} were evenly spread on Luria agar plates. Discs made of Whatman paper no. 1 (9 mm in dia) were soaked overnight in the respective composite solutions (1 mg mL^{-1}). Then, the soaked discs were placed aseptically onto the Petri plates using sterilized forceps. Tetracycline discs (10 mcg per disc) and discs soaked in sterile distilled water overnight were used as positive and negative controls, respectively. The zone of inhibition was assessed after a 12 h incubation at 37 °C following techniques outlined in previous studies.[28,46–48]

2.6.2. _In silico_ studies. _In vitro_ studies were further supported by _in silico_ analysis. Developed model structures of AlG and FeG composites were investigated for their binding affinity toward the protein targets of _Bacillus subtilis_-FtsZ, and _Escherichia coli_-GyraseB using molecular docking analysis (Autodock 4.2 programme).[49] These soil microbes are essential for decomposition, nitrogen cycling, and preserving the health of the soil.[50] These microorganisms utilize multiple mechanisms that can enhance plant growth directly, indirectly, or simultaneously. The direct mechanism involves their ability to obtain and provide essential nutrients like nitrogen, phosphorus, potassium, and minerals, as well as regulate plant hormone levels. The indirect mechanism entails the secretion of substances that act antagonistically to inhibit plant pathogens or induce resistance to pathogens in plants. As a result, these strains demonstrate effectiveness as biocontrol agents on plant tissues, preventing pathogen colonization through antibiosis against pathogens and by inducing systemic resistance in the target plant.[51] The three-dimensional coordinates of the (i) _Bacillus subtilis_-FtsZ (PDB ID: 2VAM) and

This journal is © The Royal Society of Chemistry 2024

Environ. Sci.: Water Res. Technol., 2024, **10**, 1938–1963 | **1943**

(ii) *Escherichia coli*-GyraseB (PDB ID: 6F86) crystal structures were downloaded from the Protein Data Bank.[52,53] The Swiss PDB viewer tool and ADT model were used to prepare, minimize energy, and analyze the protein structure.[54] The Lamarckian genetic algorithms were utilized for the docking process. The AlG and FeG compounds were docked with the respective protein structures, and the interaction energies and binding positions were calculated using the default parameters of Autodock. The UCSF Chimera & Pymol were used for visualization and analysis.[55,56]

3. Results and discussion

3.1. Characterization of the composites

The graphene oxide synthesized using graphite flakes by Hummer's method has been comprehensively characterized through several techniques, including SEM as depicted in Fig. S1a,† EDS (Fig. S1b†), XRD (Fig. S2a†), and FTIR (Fig. S2b†). These characterization results are available in the ESI.†

FE-SEM analysis was carried out to evaluate the morphological and textural properties of the synthesized Al-MOF, Fe-MOF, and their corresponding composites with GO (Fig. 2). The FE-SEM images of the synthesized Al-MOF and its composites exhibited a sphere-shaped morphology (Fig. 2a(i) and b(i)). The micrographs of the synthesized Fe-MOF and composites displayed uniform octahedral-shaped particles (Fig. 2c(i) and d(i)). The EDS spectra for the samples of Al-MOF, Fe-MOF, and their derived composites confirmed the existence of elements such as aluminum (Al), iron (Fe), carbon (C), and oxygen (O), with no noticeable impurities (Fig. 2(ii)).

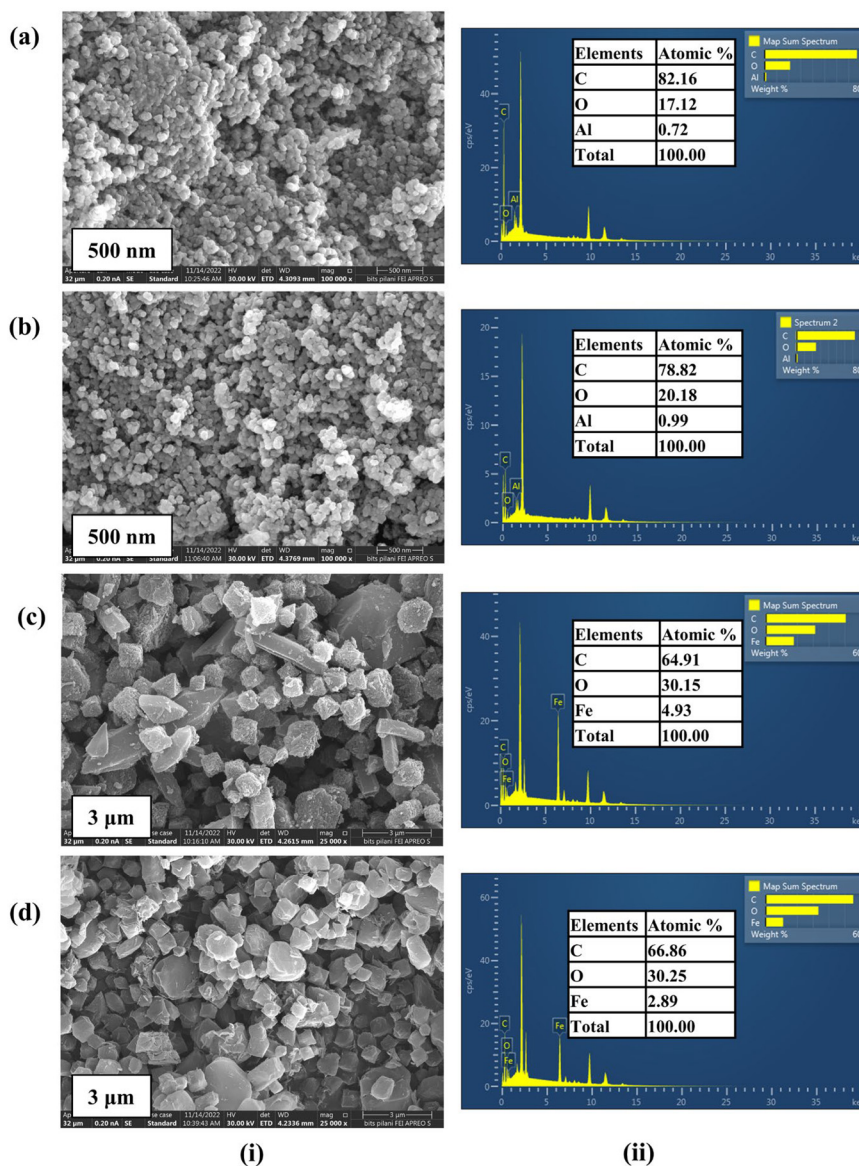**Fig. 2** (i) SEM images and (ii) EDS spectra of elemental composition of (a) Al–MOF, (b) AlGC, (c) Fe–MOF, and (d) FeGC composites.

1944 | *Environ. Sci.: Water Res. Technol.*, 2024, **10**, 1938–1963

This journal is © The Royal Society of Chemistry 2024

XRD analysis was carried out to study the change in crystallinity of the MOF particles after combination with GO and post-synthetic functionalization. The representative XRD patterns of the synthesized GO and parent Al-MOF were compared with patterns of composites and their functionalized composites (Fig. 3). It is observed that the prominent peaks of the Al-MOF at 2θ values of 9.3°, 10.2°, 15.49°, 17.12°, 18.34°, 20.97°, 25.55°, 27.68°, and 32.85° correspond to (101), (200), (011), (301), (202), (112), (312), (213), and (413) planes, respectively (Fig. 3b). The obtained XRD pattern matches precisely with the reported patterns of Al-MOFs in literature studies.[57,58] Similarly, the as-synthesized Fe-MOF exhibited characteristic peaks located at 2θ values of 8.8°, 9.41°, 18.84°, and 21.99°, corresponding to (220), (311), (511), and (852) planes, respectively (Fig. 4b). These patterns match precisely with powder Fe-MOF patterns reported in the literature.[18,19,59]

The observed XRD patterns of non-functionalized (Fig. 3c and 4c) and functionalized composites (Fig. 3d and 4d) show similar diffraction with no difference in their patterns and peak positions compared to the parent MOFs, which signifies that the crystal structure of the MOF was retained even after being combined with GO and post-synthetic
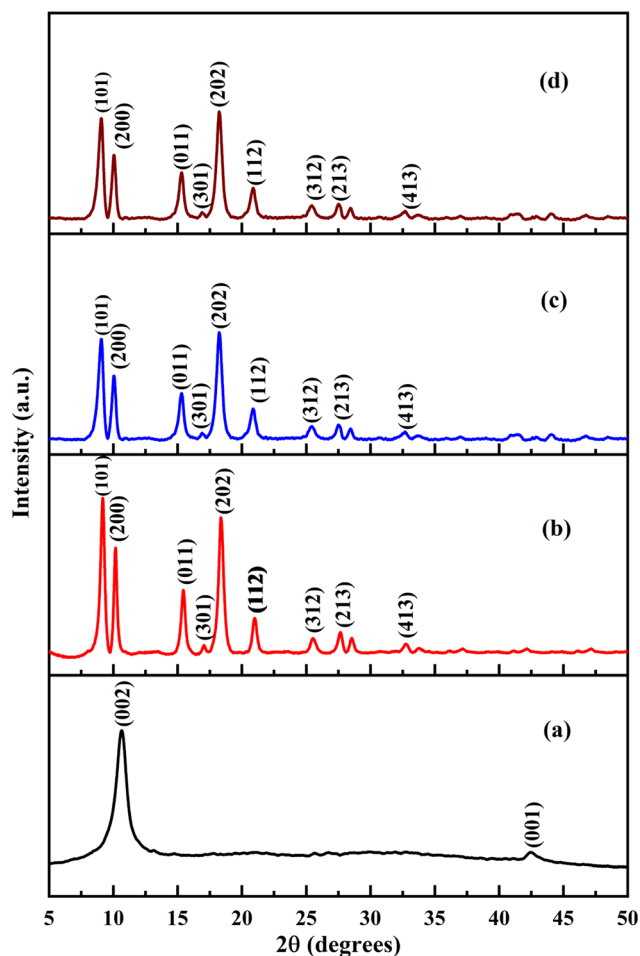

Fig. 4 XRD patterns of (a) GO, (b) Fe-MOF, (c) FeG, and (d) FeGC.
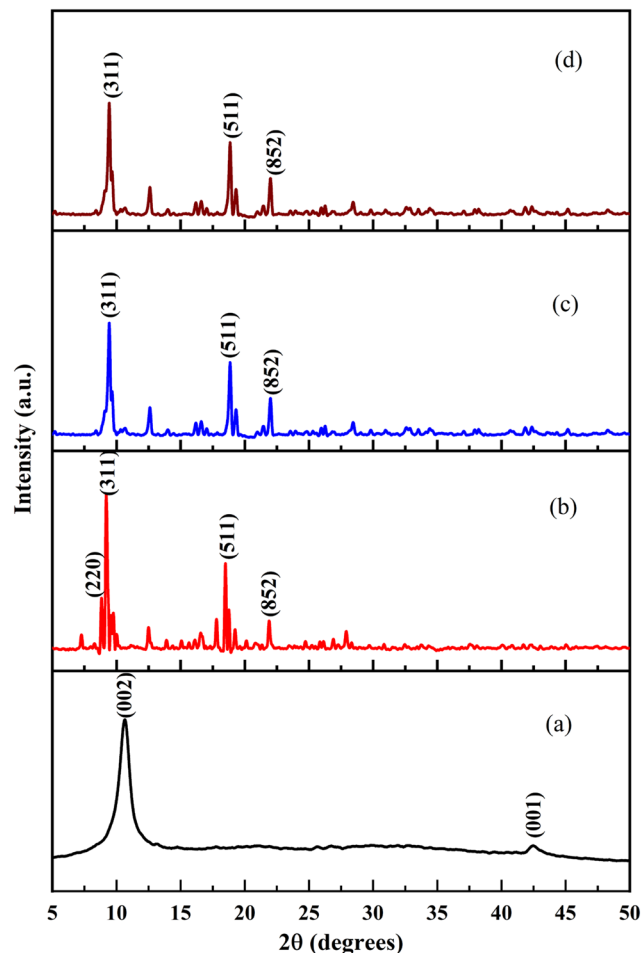

Fig. 3 XRD patterns of (a) GO, (b) Al-MOF, (c) AlG, and (d) AlGC.

functionalization. The observed XRD patterns of the composites (AlG, AlGC, FeG, and FeGC) show the disappearance of GO-associated peaks due to effective dispersion facilitated by ultrasonication, which separated the single-layer structure of GO.[59] However, the intensities of the peaks for composites (AlG, AlGC, FeG, and FeGC) were decreased. The variation in peak intensities can be attributed to covalent bonds between uncoordinated metal sites and oxygen-containing groups from the MOF and GO, respectively. This covalent bond formation enhances the stability of the composites, improving their structural integrity and mechanical strength.[14,15,63] Such stability enhancement is of paramount importance in applications related to wastewater remediation.

FTIR analysis results for the Al-MOF and its derived composites are shown in Fig. S3.† In the FTIR spectra of the Al-MOF, a broad vibration band centered at 3600–3200 cm^{-1} was observed due to the stretching of hydroxyl groups (–OH), which may be due to the surface water molecules and hydrated aluminum octahedra in the Al-MOF framework (Fig. S3b†). The peaks located at 1674 and 1510 cm^{-1} were mainly due to the stretching of a carboxyl group (C=O) for the carboxylates in the framework. The peaks at 1611 and 1510 cm^{-1} correspond

This journal is © The Royal Society of Chemistry 2024

Environ. Sci.: Water Res. Technol., 2024, 10, 1938–1963 | 1945

to asymmetric stretching, while those at 1439 and 1418 cm^{-1} are due to symmetric stretching of coordinated –COO$^-$ groups with Al metal.[60] The spectral peaks between 800–700 cm^{-1} were due to the C–H stretching of terephthalate ligands.[58,61] The absorption peaks at 600–1100 cm^{-1} are due to Al–O interactions in the Al-MOF framework.[60]

AlG and AlGC's spectra showed similar spectra to the parent Al-MOF (Fig. S3c and d†). However, a decrease in intensity was observed for the wide vibration band detected between 3600–3200 cm^{-1} when combined with graphene oxide (GO) and the organic functionalities from the MP extract. This decrease was attributed to the MOF bonding with GO and the surface modifications involving organic molecules from the extract. The new band at 1708 cm^{-1} observed in the FTIR spectrum of the functionalized composite corresponds to a carbonyl group (C=O) (Fig. S3d†). This absorption band is a characteristic peak of carbonyl compounds, including aldehydes and carboxylic acids, resulting from the incorporation of functionalities from the MG powder extract.

The FTIR spectra recorded for the Fe-MOF and its derived composites are shown in Fig. S4.† In the FTIR spectra of the Fe-MOF, the broad peak present between 3600 and 3200 cm^{-1} is related to hydroxyl groups (–OH) from surface hydration. The peaks located at 1657 and 1506 cm^{-1} were mainly due to the stretching of a carboxyl group (C=O) of the carboxylates in the framework (Fig. S4b†). The peaks at 1598 and 1388 cm^{-1} correspond to symmetric and asymmetric vibrations of O–C=O of the aromatic ring of the ligand (TPA). The bending vibration of C–H and C–O–C was observed at 746 and 1014 cm^{-1}, respectively. The characteristic peak at 549 cm^{-1} was due to Fe–O interaction in the Fe-MOF framework.[59,62] The obtained distinct peaks after combination with GO and surface functionalization are similar to those observed in the spectra of the parent Fe-MOF (Fig. S4c and d†). However, after functionalization, the peak between 3600 and 3200 cm^{-1} showed a decreased intensity and narrower broadness due to composite bonding with extract functionalities. Additionally, the peak at 1719 cm^{-1}, related to GO, completely disappeared in the FeGC composite, indicating bonding between GO surface functional groups and MOF open metal sites.

3.2. Screening of synthesized composites for their dye adsorption efficiency

The synthesized composites were screened for their maximum adsorption capacity to remove dyes (MO & MB) from wastewater (Fig. 5). The obtained results demonstrated that the Al-MOF and Fe-MOF had an adsorption capacity of 215 ± 7.1 and 347 ± 8.6 mg g^{-1} for MO and 120 ± 6.1 and 61 ± 5.1 mg g^{-1} for MB, respectively. The combination of the MOF and GO significantly improved the adsorption capacity, with enhancements of 53% and 8% for MO and 62% and 113% for MB for the composites AlG and FeG, respectively, over their parent MOF. However, after the surface
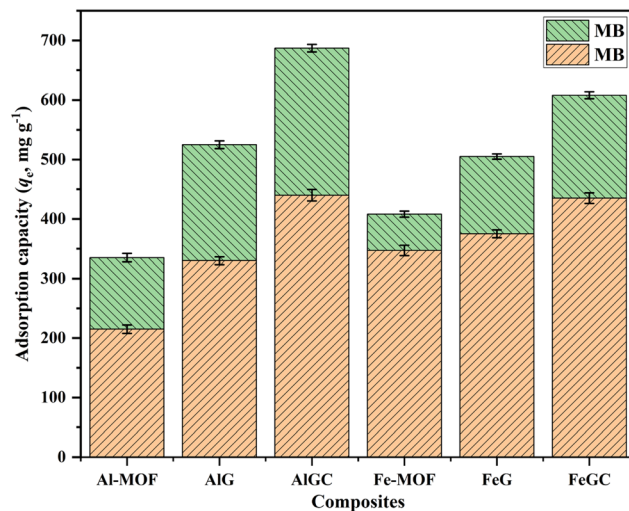

Fig. 5 Adsorption efficiency of synthesized materials for the removal of MO and MB dyes from aqueous solutions.

functionalization of the composites by MP extract, AlGC and FeGC showed an upsurge of 33% and 16% for MO and 26% and 24% for MB from their original values (uncapped). The maximum adsorption capacities for AlGC and FeGC were obtained as 440 ± 9.5 and 435 ± 8.9 mg g^{-1} for MO and 247 ± 6.3 and 173 ± 5.6 mg g^{-1} for MB, respectively. The studies concluded that AlGC and FeGC exhibited superior adsorption capacity for MO and MB dyes compared to the other tested adsorbents. It is well known that the composite's heightened surface energy resulting from the combination of the MOF with GO and the incorporation of functional groups (–COOH, –OH, etc.) on the composite surface collectively contributed to an enhanced adsorption capacity. The specific functional groups from the MP extract enhanced the adsorptive properties by increasing electrostatic forces and forming interactive bonds with the dyes.

Considering the fact that surface area and surface charge are key parameters for the higher adsorption capacity of any composite, AlGC and FeGC were further characterized by BET surface area analysis and pH$_{ZPC}$. The surface area of the composite is an essential parameter to measure the adsorption efficiency. The shape of N$_2$ adsorption & desorption isotherms and hysteresis were applied to calculate the surface area and characterization of the adsorption of AlGC and FeGC composites. The BET surface area, average pore size, Barrett–Joyner–Halenda (BJH) pore volume, and pore radius estimated for the composites are reported in Table 3. It is evident from the isotherm that the composites exhibited isotherms of type IV with a hysteresis loop of type H$_4$ (Fig. 6a and b).[63,64] The progressive increase in adsorption was observed at a relative pressure of 0–0.6 P/P_0 due to monolayer adsorbate deposition on the composite surface. Then, a steady rise in adsorption was observed at 0.6–0.9 P/P_0 due to the multi-molecular layer adsorption. The sudden rise in adsorption and desorption branch at a relative pressure of 0.9–1 P/P_0 was due to the higher number of micropores in

Table 3 Physical properties of the composites

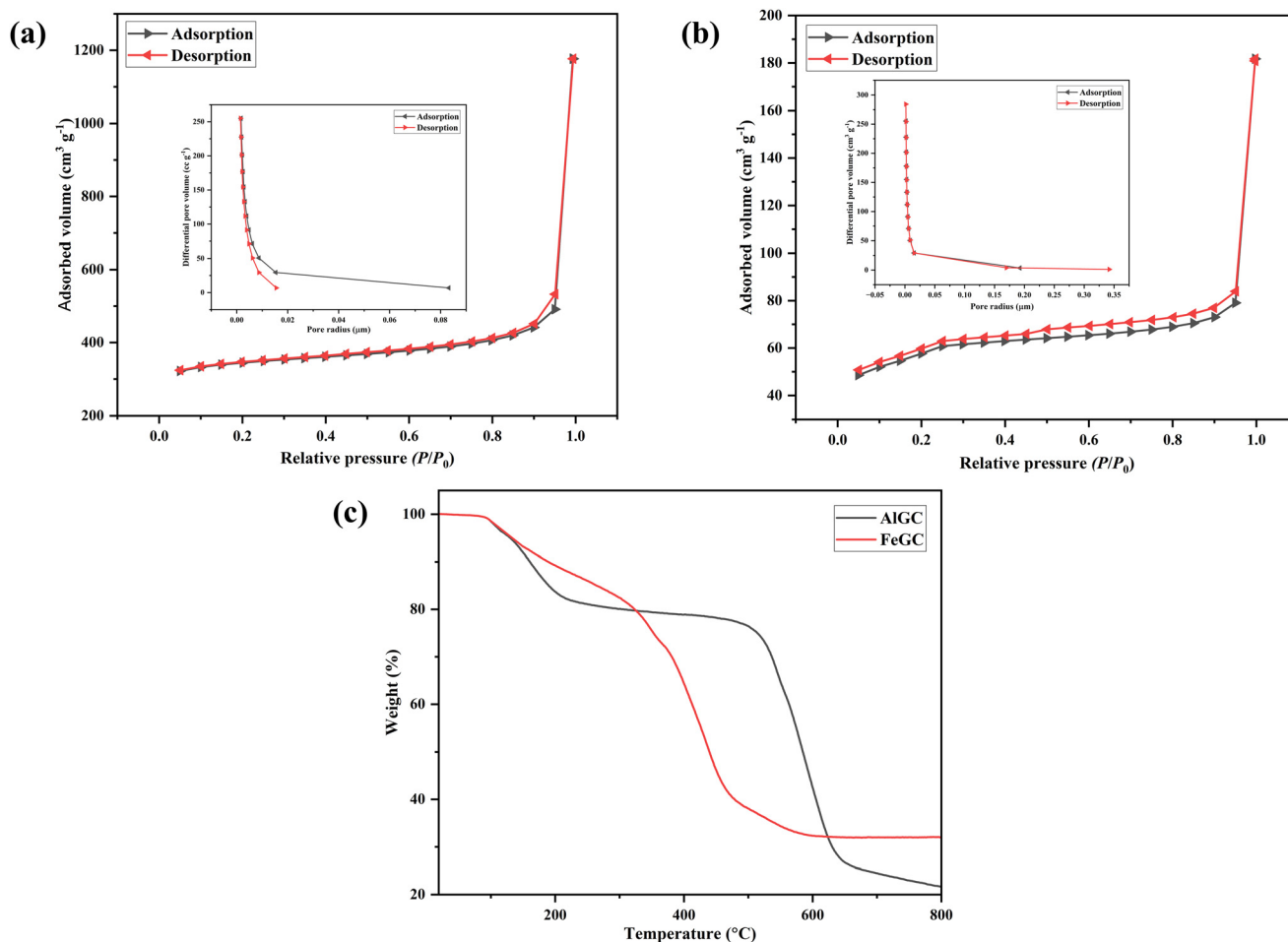| Sample	BET surface area (m² g⁻¹)	Average pore size (μm)	Pore volume (cm³ g⁻¹)	Pore radius (μm)
AlGC	1059	0.003	1.317	0.002
FeGC	189	0.002	1.191	0.002

Fig. 6 The nitrogen adsorption/desorption isotherms and BJH pore size distribution curves of (a) AlGC and (b) FeGC; (c) TGA analysis of the synthesized composites.

the composite.[64] The differences in adsorption at lower and high pressure confirm the presence of the composite, which has a significant amount of macropores and a small number of micropores. Based on the BJH method, the mesopore size distribution showed a narrow pore radius peak centered at 0.0017 μm for the composites AlGC and FeGC. The BET test results indicated that the composite's surface area (AlGC: 1059 m² g⁻¹ and FeGC: 189 m² g⁻¹) and pore volume (AlGC: 1.31 cc g⁻¹ and FeGC: 1.19 cc g⁻¹) are significantly higher, making it a promising candidate for efficient dye adsorption from wastewater. This enhancement can be attributed to the composite's formation by combining the MOF with GO.

The surface charge (pH_{ZPC}) of AlGC and FeGC was found to be 5.2 and 5.1, respectively (Fig. S5†), which corresponds to the point at which the surface charge over the composite

is neutral. It refers to the pH value at which the adsorbent surface carries no net charge.[37]

The thermal stability of AlGC and FeGC was analyzed using TGA (Fig. 6c). There was no weight loss of the composites observed up to 90 °C. The increase in temperature from 90 to 250 °C resulted in approximately 20% weight loss of composites. The composites contained water molecules of about 19 and 22 wt% for AlGC and FeGC composites, respectively. This surface moisture and other volatile compounds were easily evacuated before 250 °C. Furthermore, an increase in temperature beyond 250 °C showed the removal of residual solvent molecules entrapped within the pores of the composite.[35] The TGA curves showed 3 stages for AlGC and FeGC composites, corresponding to the removal of free and bonded H_2O molecules, followed by the

decomposition of organic ligands, and MOF decomposition at 670 and 350 °C for the AlGC and FeGC composites, respectively.[65] The TGA signifies the high thermal stability of the synthesized composites, confirming the possibility of their utilization at higher temperatures.

Further, to better understand the detailed adsorption mechanism, FTIR and XPS analysis of AlGC and FeGC was determined before and after dye adsorption. The obtained FTIR spectra after dye adsorption were compared with the recorded spectra of pure composites (Fig. 7 and 8). After dye adsorption, there was a decrease in peak intensities, a shift in spectral position, and the presence of new peaks, which confirmed the dye adsorption on the surface of AlGC and FeGC. The detailed results are discussed in section 3.6.

Fig. 9 and 10 present the XPS survey spectra of AlGC and FeGC before and after adsorption of MO and MB dyes, respectively. The full-scale XPS spectrum of composites before adsorption revealed the presence of elements in both

composites, including C 1s, O 1s, and N 1s, followed by Al 2s and Fe 2p for AlGC and FeGC, respectively. Hence, the wide range of functionalities and stable configuration achieved between the composite and graphene oxide are confirmed by XPS, corroborating the results obtained from XRD analysis. It can be observed that there was a slight shift in binding energy in the C 1s and O 1s peaks of the AlGC and FeGC composites, respectively, due to interactions between the dye molecules and the composite surface, which supported the dye molecule adsorption on the composite surface.

The results obtained from the present work and surface characteristics of the adsorbents validated the suitability of functionalized composites, *i.e.*, AlGC and FeGC, for further optimization and batch adsorption investigations to remove MO and MB dyes from synthetic aqueous solutions.

3.3. Solution pH influence on dye adsorption

Fig. 11 displays the adsorption capacity of AlGC and FeGC composites for MO and MB dyes by varying initial solution pH values (2–12). The highest MO adsorption was attained in an acidic environment, yielding 580 ± 9.8 mg g^{-1} and $470 \pm$
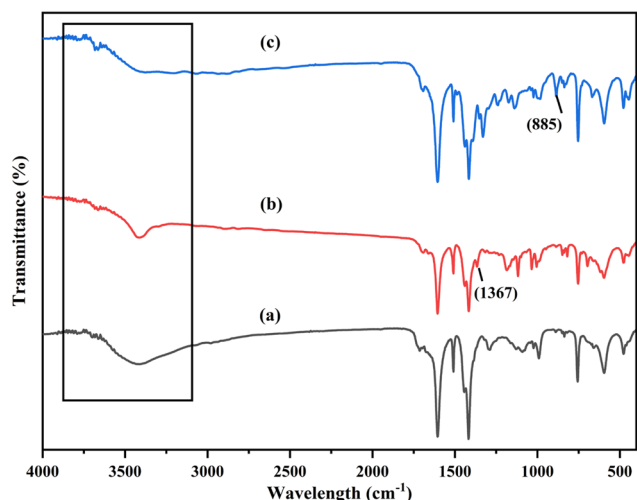

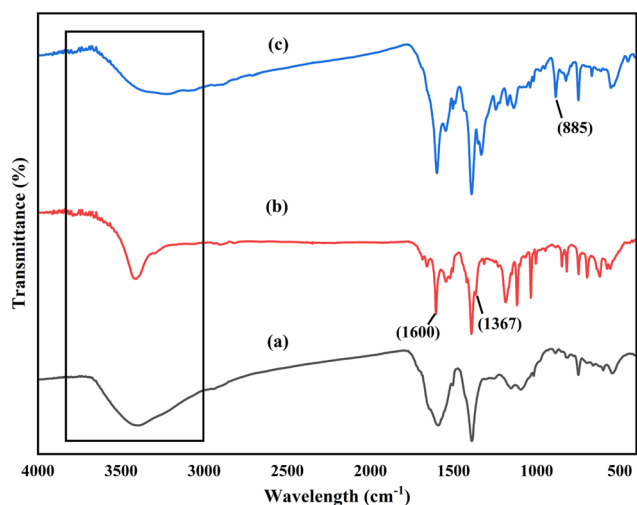**Fig. 7** FTIR spectra of (a) fresh AlGC, (b) AlGC-MO, and (c) AlGC-MB.

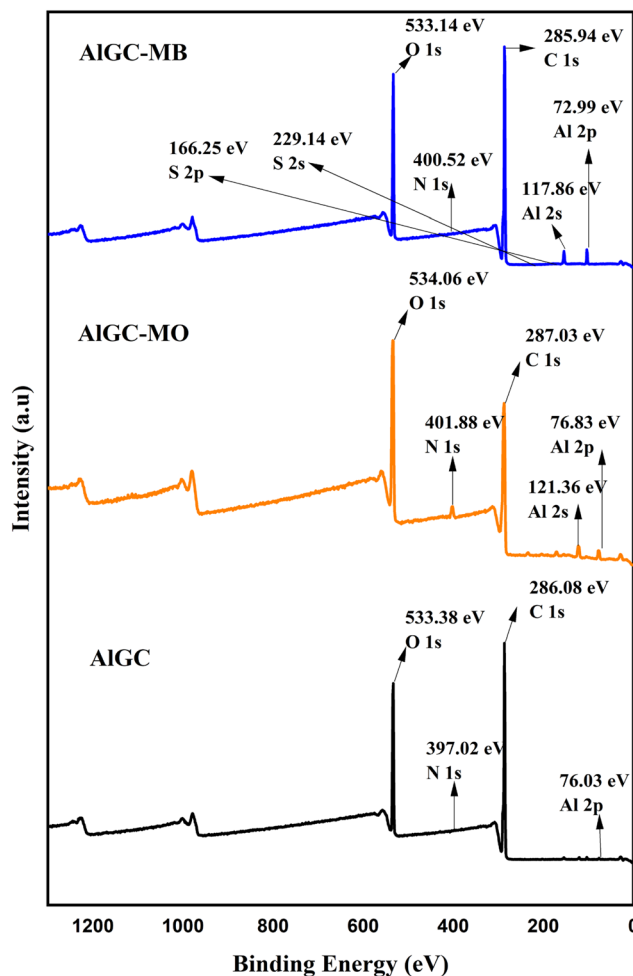**Fig. 8** FTIR spectra of (a) fresh FeGC, (b) FeGC-MO, and (c) FeGC-MB.

Fig. 9 The full XPS spectra of AlGC before and after dye adsorption.

1948 | *Environ. Sci.: Water Res. Technol.*, 2024, **10**, 1938–1963

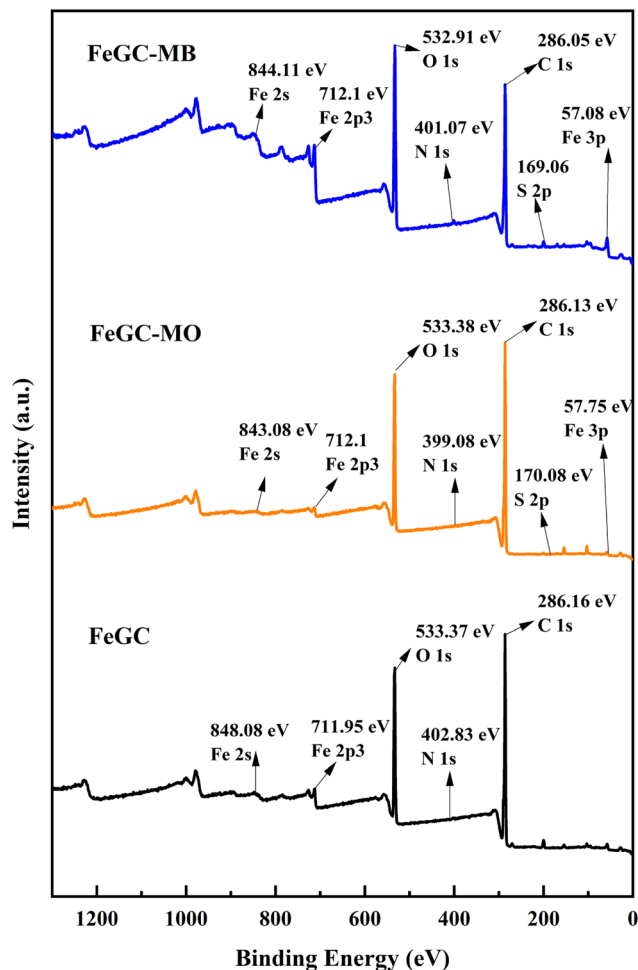This journal is © The Royal Society of Chemistry 2024

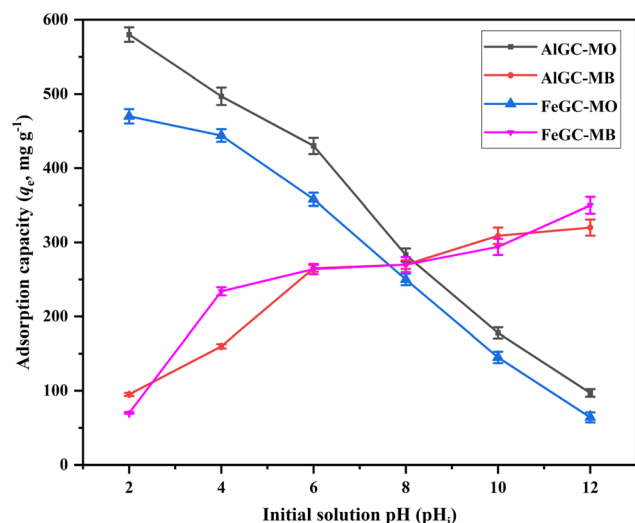**Fig. 10** The full XPS spectra of FeGC before and after dye adsorption.

Fig. 11 Influence of solution pH on dye removal using AlGC and FeGC.

9.7 mg g^{-1} using AlGC and FeGC, respectively. Conversely, maximum MB adsorption capacity values of 320 ± 10.9 and 350 ± 11.28 mg g^{-1} were achieved in the basic region using

AlGC and FeGC, respectively. At pH below pH$_{ZPC}$ of the composite (AlGC: 5.2, FeGC: 5.1), the surface is positively charged, providing an electrostatic force on the composite surface for the adsorption of the anionic dye (MO). Hence, the adsorption of MO dye reaches its maximum in the acidic region due to the favorable interaction among the negatively charged dye molecules and positively charged surface of composites.[65] Conversely, when the initial solution pH is higher than the pH$_{ZPC}$, the composite surface becomes negatively charged, making it easier for the cationic dye (MB) to adsorb.[28,37] The findings reveal that the pH level of the solution notably impacts the MO and MB adsorption onto the composite. To achieve optimal adsorption for the removal of both dyes, it is recommended to maintain a pH range between 6 and 8. The pH of the initial solutions containing MO and MB dyes was 4.4 ± 0.4 and 6.2 ± 0.3, respectively. These initial solutions were utilized without any pH adjustment to investigate the parametric effects on dye removal from wastewater using the developed composite materials. Furthermore, it should be noted that the composite surface charge properties are conducive to the specified pH conditions of the solution. Specifically, the composite exhibits positive and negative surface charges, which are suitable for the anionic (MO) and cationic (MB) dye adsorption depending on the pH conditions of the initial solution.

3.4. Optimization using the Taguchi method and statistical analysis

3.4.1. Determination of the optimum levels. Table S2† contains experimental data for the removal of dyes using synthesized composites (AlGC & FeGC), with each run corresponding to a different combination of controllable factors such as t (min), C_0 (mg L^{-1}), m (mg), and T (°C). The level five-four factor orthogonal matrix was used to collect the experimentally achieved adsorption capacity and estimation of the S/N ratio for each run. The larger S/N ratio is chosen as the primary goal of this study to optimize the dye adsorption capacity of composites.

Fig. 12 and 13 illustrate the sensitivity analysis based on the S/N ratio for the adsorption of dyes onto the developed composites by considering each input factor. These plots assist in identifying the key parameters and their ideal levels for achieving the highest adsorption capacity. Based on the S/N ratio plots (Fig. 12 and 13), the adsorption of dyes was maximum at higher C_0 (mg L^{-1}) and at a lower value of m (mg), which were found to be the most significant factors compared to other input factors. Conversely, the solution temperature and contact time had minimal effects on the composite's adsorption capacity.

Table S3† summarises the findings from the ANOVA for dye removal utilizing composites. The significance of the model and related factors were statistically validated using Fisher's test (F-test) and the coefficient of determination (R^2). The higher F-test value also confirmed that the initial dye
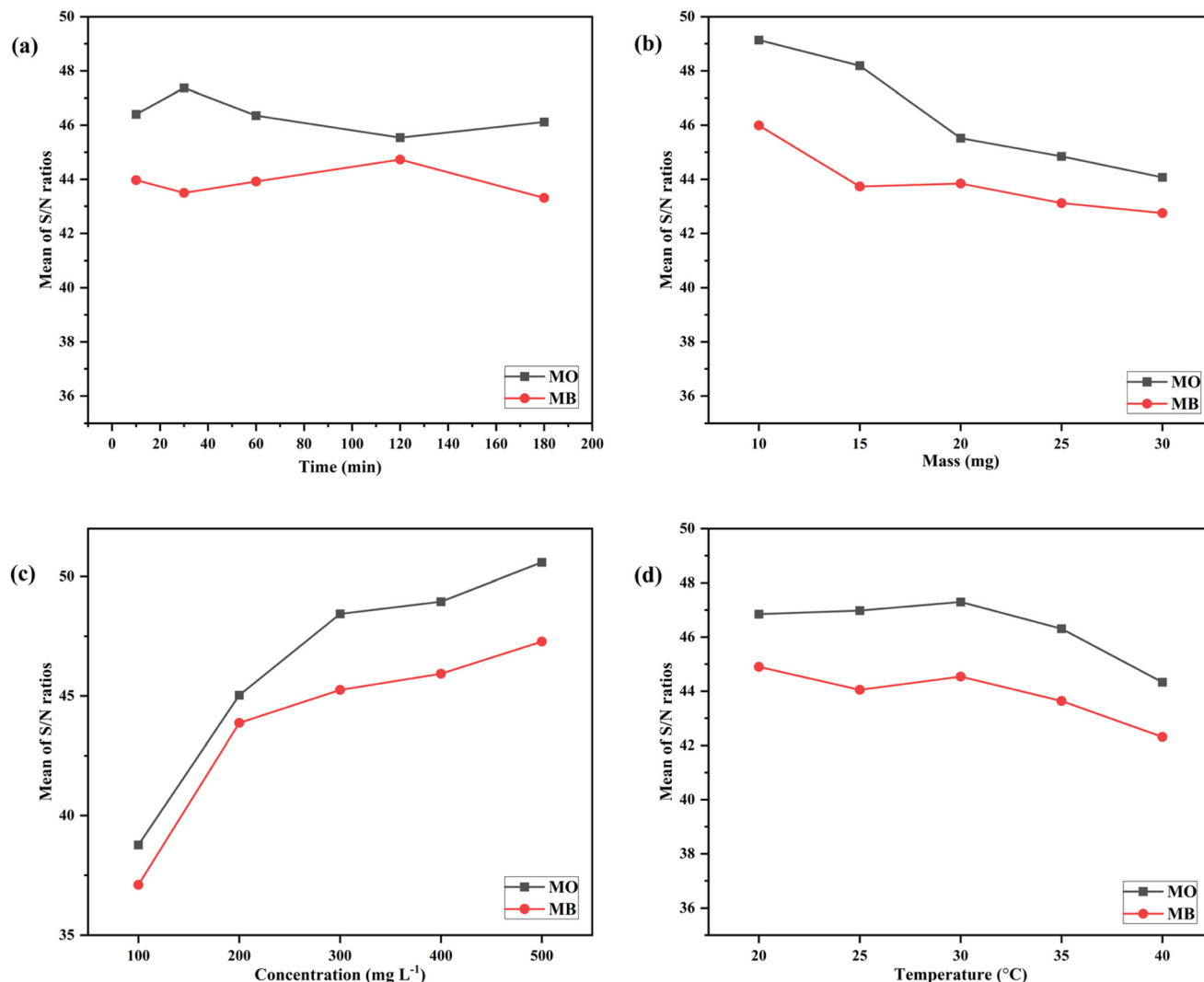
This journal is © The Royal Society of Chemistry 2024

Environ. Sci.: Water Res. Technol., 2024, **10**, 1938–1963 | **1949**

Fig. 12 Sensitivity analysis of AlGC based on S/N ratios for the parameters (a) t (min), (b) m (mg), (c) C_0 (mg L^{-1}), and (d) T (°C).

concentration and composite dosage had a more significant impact on the removal of the dye using composites than contact time and solution temperature. Moreover, the analysis revealed that the R^2 value exceeded 0.75 in all instances, suggesting that the study only accounted for 75% of the variability in the dye removal process. However, these results also suggested that the model did not account for the remaining 25% of the variance caused by the process. The study utilised percentage contribution calculations to assess the relative impact of each parameter on the process (Table 4). The findings demonstrated that among the various parameters investigated for dye removal utilizing the developed AlGC and FeGC, C_0 and m were the primary factors exerting the most influence on dye adsorption.

3.4.2. Confirmation experiments. The optimal set of parameters that can lead to the highest removal of dyes using AlGC and FeGC composites were identified based on the S/N ratio plots (Fig. 12 and 13) and are included in Table 4. At optimal parameter values, the q_{pred} of the composite for MO and MB using AlGC was estimated to be 483.29 and

294.08 mg g^{-1}, respectively, while it was 477.67 and 291.84 mg g^{-1}, respectively, using FeGC. To authenticate and affirm the model derived from Taguchi optimization, adsorption experiments were conducted at optimum parameter values utilizing AlGC and FeGC (Table 4). The study found that the predicted adsorption capacity closely matched the experimental results for MO dye removal with an error percentage of less than 13.71%. However, in the case of MB dye removal, the model significantly overestimated the predicted adsorption capacity, with an error percentage exceeding 22.62%. Hence, the study suggests that the optimization model may be employed for dye (MO & MB) removal processes using the developed composites (AlGC & FeGC).

3.5. Parametric batch studies

Taguchi optimization has provided the optimum set of factors for removing dyes from aqueous solutions using AlGC and FeGC composites. However, further batch studies were performed for the same input factors used in Taguchi

1950 | *Environ. Sci.: Water Res. Technol.*, 2024, **10**, 1938–1963

This journal is © The Royal Society of Chemistry 2024
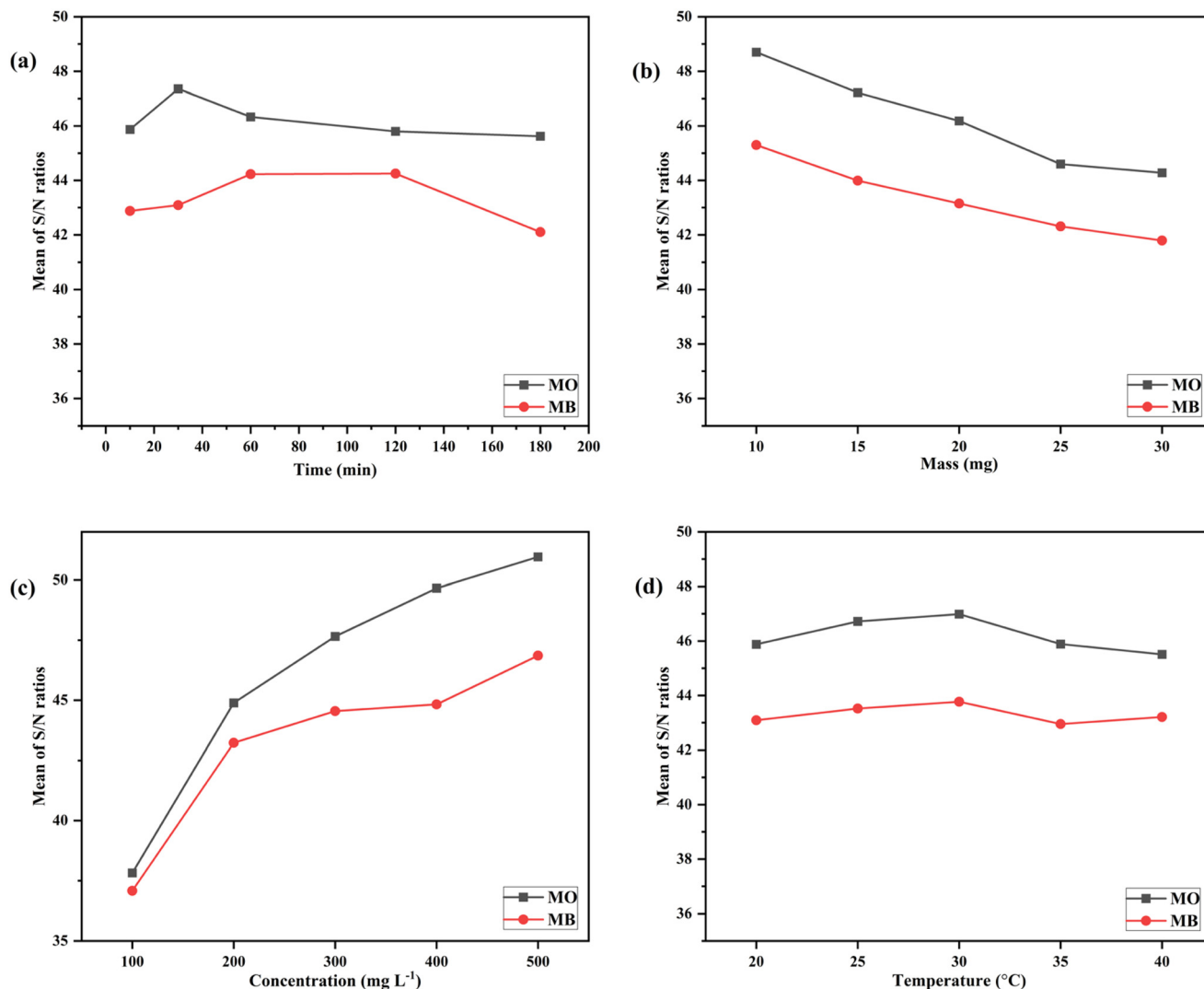
Fig. 13 Sensitivity analysis of FeGC based on S/N ratios for the parameters (a) t (min), (b) m (mg), (c) C_0 (mg L^{-1}), and (d) T (°C).

Table 4 Optimum parameter values predicted from Taguchi optimization and experimental results

Adsorbent	Dye	T (min)	m (mg)	C_0 (mg L^{-1})	T (°C)	q_{pred} (mg g^{-1})	q_{exp} (mg g^{-1})	$E\%$
AlGC	MO	30	10	500	30	483.29	425	13.71
AlGC	MB	120	10	500	20	294.08	248	18.58
FeGC	MO	30	10	500	30	477.67	435	9.81
FeGC	MB	120	10	500	30	291.84	238	22.62

optimization studies to confirm the model's adaptability to the one factor at a time (OFAAT) approach. Table 2 provides a comprehensive list of parameter values employed in the batch studies.

3.5.1. Effect of contact time. The study aimed to examine the dye adsorption rate kinetics on composites. Fig. 14a depicts the impact of contact time on the MO & MB adsorption utilizing AlGC & FeGC composites. In the initial 30 min, approximately 64% & 60% removal for MO using AlGC and 74% & 70% for MB using FeGC composites were achieved, respectively. The rapid removal at the initial stages

was attributed to wide functionalities and porous texture on the composite surface.[66] Later, the rate of dye adsorption was nearly constant with equilibrium adsorption capacities of 446 ± 14 and 414 ± 13 mg g^{-1} for MO and 233.8 ± 14 and 283 ± 7.5 mg g^{-1} for MB for the composites AlGC and FeGC, respectively, due to saturation of available active sites. The higher affinity of composites towards MO was due to the possible interaction between the acidic nature of dye and the basic properties of the composite surface, which enabled better adsorption of MO than MB. Since no appreciable change in adsorption capacity was witnessed after 120 min of

This journal is © The Royal Society of Chemistry 2024

Environ. Sci.: Water Res. Technol., 2024, **10**, 1938–1963 | **1951**

Fig. 14 Investigating the influence of (a) t (min), (b) C_0, (mg L^{-1}), (c) T (°C), and (d) m (mg L^{-1}) on MO and MB adsorption using AlGC and FeGC.
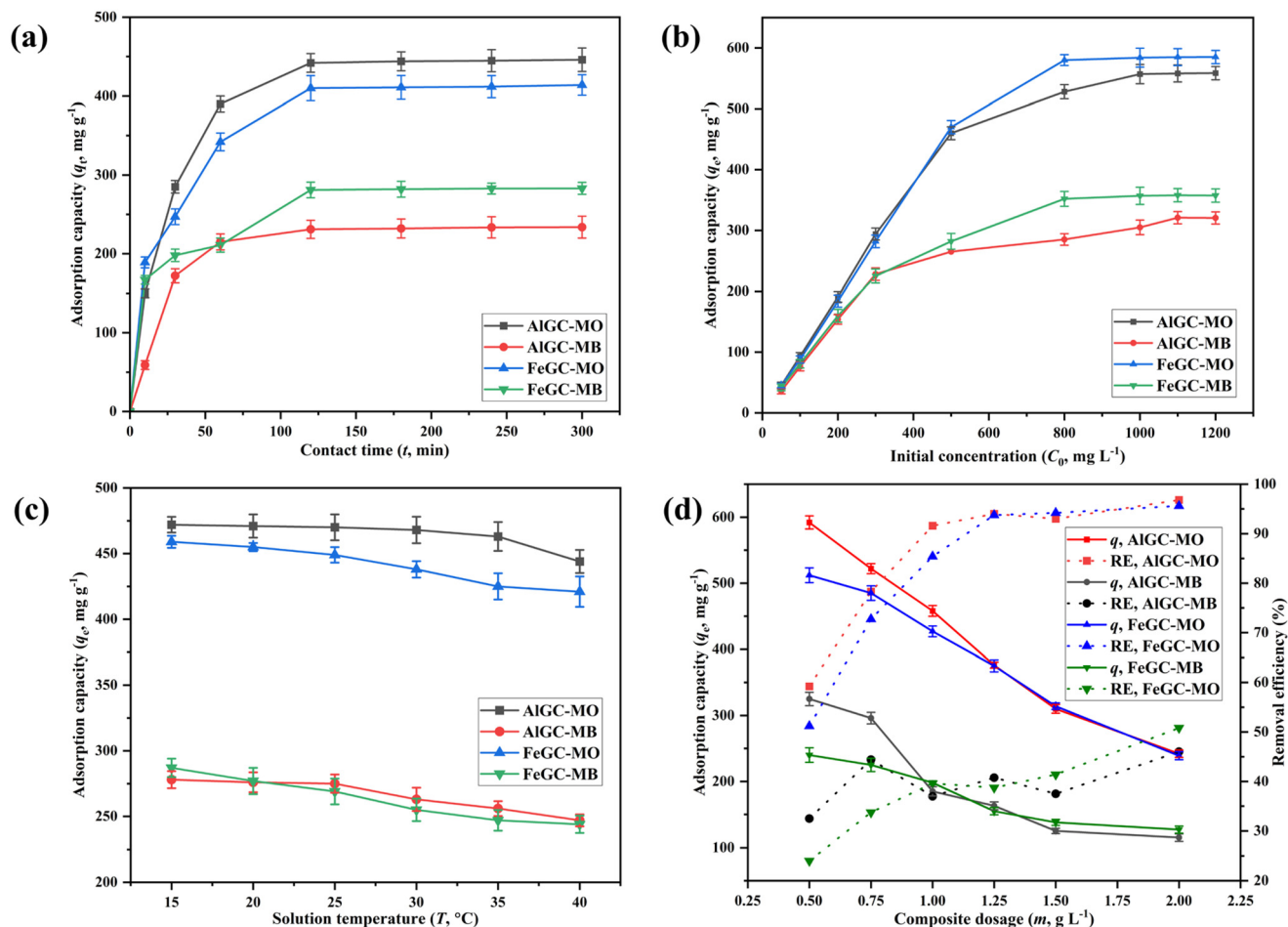
contact time, hence, the equilibrium adsorption time for maximum dye removal was considered as ~120 min, which is the same as the equilibrium adsorption time predicted from the Taguchi optimization.

Indeed, adsorption time studies alone may not fully elucidate the complex interaction between the dye and composite. Therefore, it is necessary to employ appropriate models to analyze this interaction comprehensively. The present study utilized non-linear forms of kinetic models to determine the removal rate and other kinetic parameters of dye removal using AlGC and FeGC. The Origin software 2023 (Learning version) was utilized to conduct non-linear adsorption kinetic model fitting using the experimental kinetic data (Fig. S6 and S7†). The estimated kinetic constants and parameters by fitting the experimental results to the kinetic models are reported in Tables 5 and 6.

The experimental kinetic data of dye adsorption using AlGC demonstrated strong concordance with the pseudo-first-order kinetic model, yielding an $R^2 > 0.99$ (Tables 5 and 6). The estimated equilibrium adsorption capacity (q_e, mg g^{-1}) was 448 ± 3.8 & 234 ± 14 mg g^{-1} for MO and MB removal, respectively, using AlGC that is well-concordant with the experimentally obtained adsorption capacities of dyes

(MO: 446 ± 14 mg g^{-1} and MB: 233.8 ± 14 mg g^{-1}). Therefore, the adsorption of dyes by AlGC is more likely a physical adsorption process.

Similarly, the observed kinetics of dye adsorption using FeGC closely adhere to the pseudo-second-order kinetic model, exhibiting higher R^2 values (MO: 0.98 and MB: 0.95) compared to the R^2 values obtained for the first-order kinetic model (Tables 5 and 6). However, the estimated q_e values (MO: 407 ± 14 mg g^{-1} and MB: 266 ± 14 mg g^{-1}) from the first-order kinetic model provided close estimation with the experimentally obtained adsorption capacities (MO: 414 ± 13 mg g^{-1} and MB: 283 ± 7.5 mg g^{-1}) using FeGC. Hence, the consistent experimental applicability of the first-order kinetic model shows the presence of physisorption as the primary adsorption process; however, chemisorption can't be denied. In addition, the calculated rate constants (k_1 and k_2) from the first- and second-order kinetic models demonstrated that the adsorption of dyes by AlGC and FeGC occurs rapidly, reaching saturation within a short time.

The Elovich kinetic model is considered a better method for describing the adsorption rate kinetics than the commonly used pseudo-first and second-order rate kinetic models. The Elovich model provides a more comprehensive

Table 5 Predicted isotherm and kinetic parameters and constants for dye adsorption on the AlGC composite

Model	Parameters	Values		Regression coefficient (R^2)	
		MO	MB	MO	MB
Kinetic models					
Pseudo-first-order	q_e (mg g^{-1})	448 ± 3.8	234 ± 4	0.998	0.992
	k_1 (min^{-1})	0.036 ± 0.006	0.039 ± 0.003		
Pseudo-second-order	q_e (mg g^{-1})	493 ± 11	260 ± 12	0.991	0.967
	k_2 (g mg^{-1} min^{-1})	$9.95 \times 10^{-4} \pm 1 \times 10^{-5}$	$1.95 \times 10^{-4} \pm 5 \times 10^{-5}$		
Elovich model	α (mg g^{-1} min^{-1})	67 ± 36	34 ± 27	0.956	0.912
	β (g mg^{-1})	0.011 ± 0.001	0.021 ± 0.004		
Isotherms					
Langmuir	Q_m (mg g^{-1})	577 ± 37	336 ± 13	0.91	0.97
	b (L mg^{-1})	0.061 ± 0.018	0.017 ± 0.003		
	R_L	1–0.013	1–0.04		
Freundlich	$1/n$	0.24	0.29	0.77	0.85
	K_F (mg g^{-1}) (dm^3 mg^{-1})$^{1/n}$	123 ± 41	45 ± 15		
Temkin isotherm	A_T (L min^{-1})	1 ± 0.6	0.19 ± 0.06	0.87	0.95
	B (J mol^{-1})	91 ± 13	64 ± 5		
	b_T	26.97	38.28		
D–R isotherm	Q_m (mg g^{-1})	532 ± 34	297 ± 10	0.88	0.96
	K (mol^2 kJ^{-2})	$1 \times 10^{-5} \pm 2 \times 10^{-6}$	$1.8 \times 10^{-4} \pm 3 \times 10^{-5}$		
	E (J mol^{-1})	219.26	52.27		

Table 6 Predicted isotherm and kinetic parameters and constants for dye adsorption on the FeGC composite

Model	Parameters	Values		R^2	
		MO	MB	MO	MB
Kinetic models					
Pseudo-first-order	q_e (mg g^{-1})	407 ± 14	266 ± 14	0.961	0.895
	k_1 (min^{-1})	0.037 ± 0.006	0.066 ± 0.001		
Pseudo-second-order	q_e (mg g^{-1})	445 ± 14	288 ± 12	0.981	0.956
	k_2 (g mg^{-1} min^{-1})	$1.28 \times 10^{-4} \pm 2 \times 10^{-5}$	$3.44 \times 10^{-4} \pm 1 \times 10^{-5}$		
Elovich model	α (mg g^{-1} min^{-1})	94 ± 43	238 ± 157	0.975	0.979
	β (g mg^{-1})	0.013 ± 0.001	0.02 ± 0.003		
Isotherms					
Langmuir	Q_m (mg g^{-1})	631 ± 42	387 ± 7	0.92	0.99
	b (L mg^{-1})	0.036 ± 0.01	0.016 ± 0.001		
	R_L	1–0.02	1–0.04		
Freundlich	$1/n$	0.28	0.31	0.76	0.92
	K_F (mg g^{-1}) (dm^3 mg^{-1})$^{1/n}$	106 ± 41	47 ± 12		
Temkin isotherm	A_T (L min^{-1})	0.43 ± 0.2	0.22 ± 0.03	0.88	0.98
	B (J mol^{-1})	114 ± 15	72 ± 3		
	b_T	21.66	34.40		
D-R isotherm	Q_m (mg g^{-1})	589 ± 11	337 ± 17	0.99	0.92
	K (mol^2 kJ^{-2})	$4 \times 10^{-5} \pm 3 \times 10^{-6}$	$2 \times 10^{-4} \pm 6 \times 10^{-5}$		
	E (J mol^{-1})	105.23	49.78		

description of the adsorption process by incorporating two rate constants. These constants are useful in characterizing the initial rapid adsorption phase, followed by a slower adsorption rate as the surface becomes saturated. The adsorption rate (α, mg g^{-1} min^{-1}) and desorption rate (β, g mg^{-1}) were calculated by fitting the non-linear Elovich model to the experimental kinetic data for the dye adsorption (Fig. S6, S7† and Tables 5, 6). This investigation showed that the adsorption rate was greater than the desorption rate since the values of α for removal of both dyes utilizing the composites were higher than the β values.[67] The lower desorption rate suggested that the synthesized composite provides better removal efficiency of the dyes.

3.5.2. Effect of concentration. Decolorizing dyes is an essential process in various sectors as it effectively prevents the continuous release of wastewater containing colors into the environment. Utilizing AlGC and FeGC, the study investigated the effect of initial dye concentration on dye adsorption, and the obtained results are presented in Fig. 14b. The direct correlation between the initial dye concentration and the adsorption capacity was observed. The adsorption capacity reached a peak of 558 ± 11 and 585 ± 9 mg g^{-1} for MO and 320 ± 10 and 357 ± 10.9 mg g^{-1} for MB using AlGC and FeGC, respectively, as the concentration of the dye increased up to 800 and 1000 mg L^{-1} for MO and 1100 and 800 mg L^{-1} for MB. This increase was mainly due

This journal is © The Royal Society of Chemistry 2024

Environ. Sci.: Water Res. Technol., 2024, **10**, 1938–1963 | 1953

to a higher initial dye concentration, which resulted in an increase in driving force and rate of mass transfer during dye removal using the composite.[68] However, the value of adsorption capacity climbed slightly and reached a plateau with an increase in dye concentration beyond 800 mg L^{-1}. The absence of a substantial rise can be attributed to the decrease in the proportion of active sites on the composite compared to the number of dye molecules in the solution at higher concentrations. This leads to the complete utilization of active sites and the establishment of an equilibrium.[66]

Further, the study utilized four different types of non-linear isotherms (Langmuir, Freundlich, D–R, and Temkin) to fit the experimental equilibrium studies of dye adsorption by the composites (Fig. S8 and S9†) and obtained parameters are presented in Tables 5 and 6. The results obtained from isotherm models aid in comprehending the interaction between the dye molecules and the AlGC and FeGC surface. Among the Langmuir and Freundlich isotherms, the Langmuir isotherm proved to be the most suitable fit for the equilibrium data. It exhibited an r^2 exceeding 0.9 for both MO and MB adsorption on both composites, confirming that dye molecules cover the composites' surface in a monolayer. The maximum adsorption capacity from the Langmuir model was obtained as 577 ± 37 and 631 ± 42 mg g^{-1} for MO and 336 ± 13 and 387 ± 7 mg g^{-1} for MB using AlGC and FeGC, respectively, which showed a good match with the experimentally obtained adsorption capacity. The separation constant R_L, falling within the range of 0–1, indicates favorable adsorption of the dyes on the composites.[69] Additionally, the adsorption parameters, adsorption intensity $(1/n)$ and adsorption capacity (K_F), calculated from the Freundlich isotherm, confirmed the feasibility and favorability of dye adsorption on the AlGC and FeGC surfaces. Successful favourable adsorption required a value of $1/n$ in the range of 0–1, which was achieved by the adsorption of dyes onto the AlGC and FeGC composites. The higher K_F values obtained for adsorption of dyes onto the synthesized composites indicated a faster adsorption rate, demonstrating the applicability for commercial utilization.[67]

The isotherms, such as Langmuir and Freundlich, were inaccurate in differentiating between the types of the adsorption process, whether chemical or physical, as they assume constant adsorption potential.[70] Therefore, it is necessary to include Temkin and D–R isotherms to examine the adsorption process type. The higher adsorption affinity (Q_m) values obtained from fitting experimental data to these models indicated that the developed composites had a greater affinity towards removing the dyes. The values of the adsorption intensity E and B obtained from the Temkin and D–R isotherms were less than 219 J mol^{-1}, signifying that the dye removal using the developed composites involved a physical adsorption process.[37] The obtained parameters from isotherms would be beneficial for the design of large-scale applications.

3.5.3. Effect of temperature. The influence of temperature on the adsorption of dyes onto composite surfaces is depicted in Fig. 14c. It is important to note that temperature plays a crucial role in scaling the adsorption process. As the temperature rose from 15 to 40 °C, there was a slight reduction in adsorption capacity. For AlGC, the decline was from 472 ± 5 to 444 ± 8 mg g^{-1} for MO and from 278 ± 6.5 to 247 ± 4.5 mg g^{-1} for MB. Similarly, for FeGC, the drop was from 459 ± 4 to 421 ± 11 mg g^{-1} for MO and from 287 ± 6.9 to 244 ± 6.5 mg g^{-1} for MB. This decreasing trend of adsorption capacity suggested the exothermic behavior of dye adsorption on composite surfaces. Extended exposure of dye molecules to elevated temperatures increases their kinetic energy, diminishing adsorption capacity and weakening interactions with the AlGC & FeGC active regions.[28] Therefore, using the developed composites, it is recommended to use a lower solution temperature in the range of 15–25 °C for the adsorption of MO and MB.

To evaluate dye removal using composites and understand its underlying mechanism, it was essential to determine thermodynamic parameters, including entropy $(\Delta S°)$, enthalpy $(\Delta H°)$, and Gibbs free energy $(\Delta G°)$. Understanding these parameters is essential for designing large-scale systems and provides valuable insights into the energy changes associated with adsorption. The thermodynamic parameters can be calculated by applying van 't Hoff and Gibbs's free energy equations.[37] The experimental results gathered across solution temperatures ranging from 15 to 40 °C were linearly fitted to the van 't Hoff equation (Fig. S10 and S11†), and the resulting parameters are shown in Table 7. Negative $\Delta H°$ values of −19.54 and −7.75 kJ mol^{-1} were observed for MO and MB removal, respectively using AlGC, while −24.25 and −11.00 kJ mol^{-1} were observed for MO and MB removal, respectively using FeGC. These values collectively indicated that the dye removal process using AlGC and FeGC was exothermic and followed physical adsorption. The estimated standard entropy $\Delta S°$ was negative for both dyes' adsorption on the developed composites, demonstrating the reversibility of the adsorption process and the decrease in the degree of randomization at the solid–liquid interface as temperature increased.[70,71]

The negative value of Gibbs free energy $(\Delta G°)$ within the temperature ranges affirming the dye adsorption process is highly favorable and spontaneous. However, with increased temperature, the adsorption process was unfavorably impacted, favoring desorption and reducing its spontaneity. This is explained by the rise in $\Delta G°$ values, and an associated reduction in equilibrium constant (K_C) values.[28,72] Overall, thermodynamic studies show the higher affinity of dye molecules at lower temperatures for dye adsorption utilizing the developed composites.

3.5.4. Effect of composite dosage. The composite dosage evaluation is crucial to estimate the trade-off between the percentage removal and the adsorption capacity of dyes. A study was conducted to observe the impact of varying composite dosages on dye adsorption capacity and removal efficiency (Fig. 14d). The results showed that at an increase in the composite dosages within the solution ranging from 0.5 to 2 g L^{-1}, the adsorption capacity of dyes was found to

1954 | *Environ. Sci.: Water Res. Technol.*, 2024, **10**, 1938–1963

This journal is © The Royal Society of Chemistry 2024

Table 7 Constants of equilibrium and thermodynamic parameters for dye removal from AlGC and FeGC composites

	T (°C)	q_e (mg g^{-1})	K_c	$\Delta G°$ (kJ mol^{-1})	$\Delta S°$ (J mol^{-1} K^{-1})	$\Delta H°$ (kJ mol^{-1})	R^2
AlGC							
MO	15	472	16.85	−7.09	−43.23	−19.54	0.67
	20	471	16.24	−6.87			
	25	470	15.66	−6.66			
	30	468	14.62	−6.44			
	35	463	12.51	−6.23			
	40	444	7.928	−6.01			
MB	15	278	1.25	−0.81	−24.11	−7.75	0.89
	20	276	1.23	−0.69			
	25	275	1.22	−0.57			
	30	263	1.10	−0.45			
	35	256	1.04	−0.33			
	40	247	0.97	−0.20			
FeGC							
MO	15	459	11.19	−6.05	−63.18	−24.25	0.79
	20	455	10.11	−5.73			
	25	449	8.80	−542			
	30	438	7.06	−5.10			
	35	425	5.66	−4.79			
	40	421	5.32	−4.47			
MB	15	287	1.34	−0.71	−35.75	−11.00	0.97
	20	277	1.24	−0.53			
	25	269	1.16	−0.35			
	30	255	1.04	−0.17			
	35	247	0.97	0.004			
	40	244	0.95	0.18			

drop by more than 60% from their maximum adsorption capacity (at m = 0.5 g L^{-1}) of 592 ± 9.8 & 512 ± 11.2 mg g^{-1} for MO and 325 ± 10.1 & 240 ± 11 mg g^{-1} for MB using AlGC and FeGC, respectively. This phenomenon can be attributed to the concentration gradient between the composite and dye molecules.[73] However, as the composite dosage increased from 0.5 to 2 g L^{-1}, the removal percentage increased from 59.2 to 96.8% & 51.2 to 95.6% for MO, and 32.5 to 46% & 24 to 50.8% for MB using AlGC and FeGC, respectively. This increase in removal percentage can be attributed to the availability of more active sites for the adsorption for the fixed number of dye molecules present in the solution.[28]

3.6. The plausible adsorption mechanism of dye on the composite

The GO–MOF composite modified by MP extract has a diverse range of functional groups (–OH, –COOH, C=O) and metal sites (uncoordinated Fe^{3+} and Al^{3+}), which may facilitate the dye removal through hydrogen bonding, van der Waals force, π–π interaction, and intense interaction bond creation between the dye molecule and the composite surface.[74,75] To delve deeper into understanding the adsorption mechanism, XPS analysis was employed to verify the changes in AlGC and FeGC before and after dye adsorption. After adsorption, the interactions between the dye molecules and the composite surface can be seen to have caused a modest shift in binding energy in the C 1s and O 1s peaks of the AlGC and FeGC composites, respectively (Fig. 9 and 10). The observed shifts in peak positions suggest that the chemical bonding between the dye molecules and the

composite material may involve electrostatic, hydrogen bonding, and π–π interactions, potentially leading to substantial alterations.[76] In addition, the data also showed a change in the N 1s peaks and the emergence of S 1s peaks, indicating the successful binding of dye molecules to the composite material. Moreover, the involvement of metallic elements in the adsorption of dye molecules was detected (Fig. 9 and 10). A noticeable change in binding energy and the appearance of new peaks associated with the metallic elements indicate alterations in the chemical states of these specific elements after dye adsorption.[76] The schematic representation of probable sorption mechanisms for the adsorption of the dyes on the AlGC and FeGC surface is shown in Fig. 15. The findings from the analysis of adsorption kinetics and isotherms indicated the physical adsorption of dyes on AlGC and FeGC. Moreover, the adsorption of dyes is predominantly influenced by the solution's pH level and the composite's surface charge, which is dictated by the surface functional groups.

The changes associated with the dye molecules' adsorption on the composite surface were analyzed by FTIR spectroscopy (Fig. 7 and 8). The obtained spectra after dye adsorption were compared with the recorded spectra of pure composites and some distinct changes were observed after dye adsorption. The broad and highly intense peak observed between 3600 and 3200 cm^{-1} before dye adsorption was changed to a less intense peak with a shift in spectral position due to the overlapping of dye molecules and participation of H-bonding in the adsorption process.[77] The new peaks at 1367 cm^{-1} and 1600 cm^{-1} after MO adsorption are due to the SO$_3^-$ and phenyl groups, suggesting the possible electrostatic and n–π

This journal is © The Royal Society of Chemistry 2024

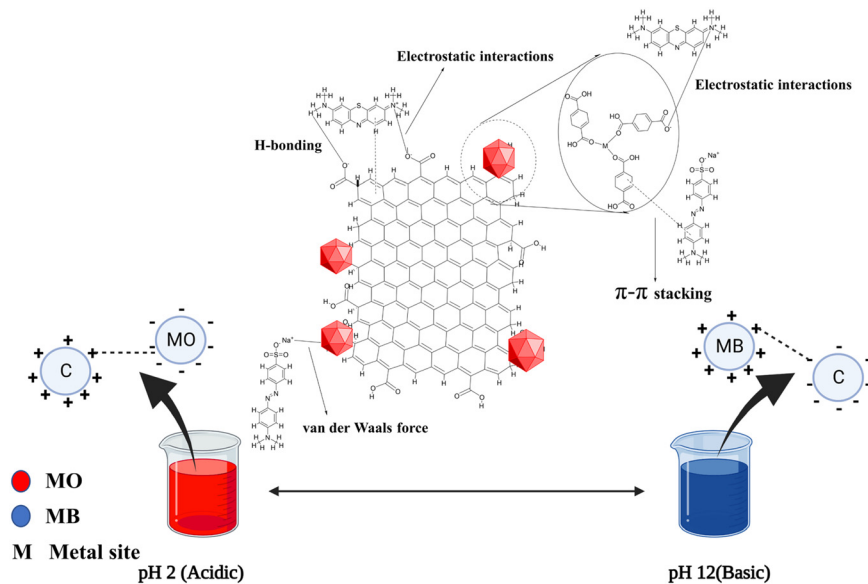*Environ. Sci.: Water Res. Technol.*, 2024, **10**, 1938–1963 | **1955**

Fig. 15 Elucidating plausible mechanisms for the dye molecule adsorption on composite structures.

interaction between the composite and MO.[78] After MB adsorption, the slight change in intensity and frequency of the band related to –OH groups (3600–3200 cm^{-1}) resulted from the bonding of surface hydroxyl groups present on the composite with the N atoms of the MB dye molecules. The new peak at 885 cm^{-1} was related to hydrogen bonding between the dye molecules and composite.[79] In addition, the new peaks and changes in spectra frequencies confirmed the dye molecules' adsorption on the composite surface.[77]

3.7. Competitive adsorption studies

Typically, numerous dyes are present in textile industry effluents, and because dyes may compete with one another, thus the performance of developed composites might vary considerably in the presence of more than one dye. Investigating the composite's selectivity toward particular dyes present in the effluent is crucial. Among the tested dyes, the highest adsorption capacity was observed for MO, with a value of 64 ± 5 and 125.17 ± 9 mg g^{-1}, followed by 15 ± 2.5 and 87.31 ± 6 mg g^{-1} for MB using AlGC and FeGC, respectively, in a binary system of MO and MB.

However, a distribution coefficient (K_d) is required to comprehend the competitive adsorption between these dyes in the solution. The K_d value can be approximated by comparing the dye concentration in the solid phase to that in the equilibrium solution, which can be calculated using eqn (3).

$$K_d = \frac{C_0 - C_f}{C_f}\left(\frac{v}{m}\right) \tag{3}$$

where K_d represents the distribution coefficient in L g^{-1}, and the estimated K_d from the experimental results was 0.34 and 0.99 L g^{-1} for MO and 0.06 and 0.53 L g^{-1} for MB using AlGC and FeGC, respectively. These findings indicated that the

developed composites demonstrated higher selectivity towards MO adsorption than MB in a binary system.

3.8. Regeneration studies

The efficacy of a composite saturated with dye molecules was evaluated through adsorption–desorption experiments using an acid–solvent mixture as a regenerating agent. Literature studies have revealed that the combination of acid and ethanol mixture effectively removes cationic and anionic dyes from the composite surface.[80] The reusability of the composite was tested through five successful adsorption–desorption cycles (Fig. 16). Despite the slight drop observed in removal efficiency after the first cycle (<20%), the regenerated composite continued to display ~50% removal efficiency towards dyes at the 5th adsorption–desorption cycle. The results from the adsorption–desorption experiments indicated that the composite could be regenerated and reused multiple times, making it an economical and promising material for industrial applications.

3.9. Environmental toxicity studies

The rapid progress in composite synthesis and its release into the environment without being tested for its antimicrobial and toxic effects has led to rising environmental concerns. Therefore, it is highly relevant to determine the toxic effects of composites on various soil microbes.

3.9.1. *In vitro* studies. The effect of composites on the persistence of the studied bacterial species (*E. coli* and *B. subtilis*) is shown in Table 8. According to the obtained results, no substantial deterrent was observed in bacterial growth in the presence of AlGC and FeGC compared to the control.

Furthermore, the assay demonstrated that, in contrast to the positive control (antibiotics) and the negative control
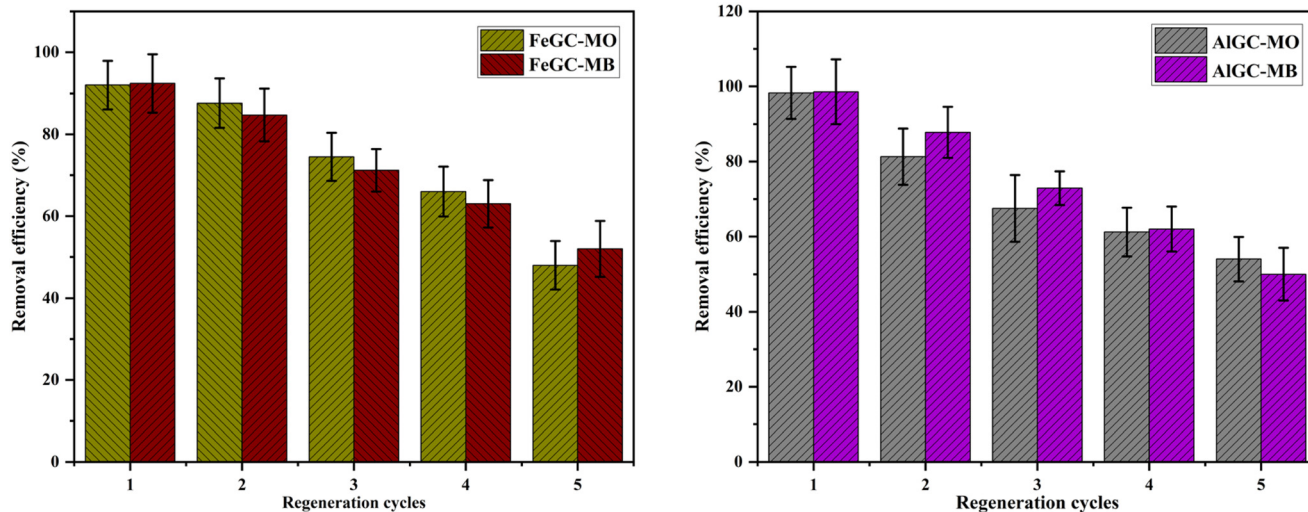
Fig. 16 Performance of composites for MO and MB dye removal up to five regeneration cycles.

Table 8 Bacterial viability analysis in the presence of AlGC and FeGC

Sample	$E.\ coli$ cell count (CFU mL^{-1})		Sample	$B.\ subtilis$ cell count (CFU mL^{-1})	
	Initial	After 12 h of treatment		Initial	After 12 h of treatment
Control	$\sim27.8 \times 10^8$	$\sim132 \times 10^9$	Control	$\sim51 \times 10^7$	$\sim65 \times 10^8$
AlGC	$\sim27.8 \times 10^8$	$\sim127 \times 10^9$	AlGC	$\sim51 \times 10^7$	$\sim58 \times 10^8$
FeGC	$\sim27.8 \times 10^8$	$\sim129 \times 10^9$	FeGC	$\sim51 \times 10^7$	$\sim68 \times 10^7$

(sterile distilled water), the examined bacterial and fungal species did not exhibit any zone of inhibition (Fig. 17). Therefore, based on the obtained results, it can be inferred that the composites had no detrimental effect on the ecologically significant soil microorganisms.[28,81]

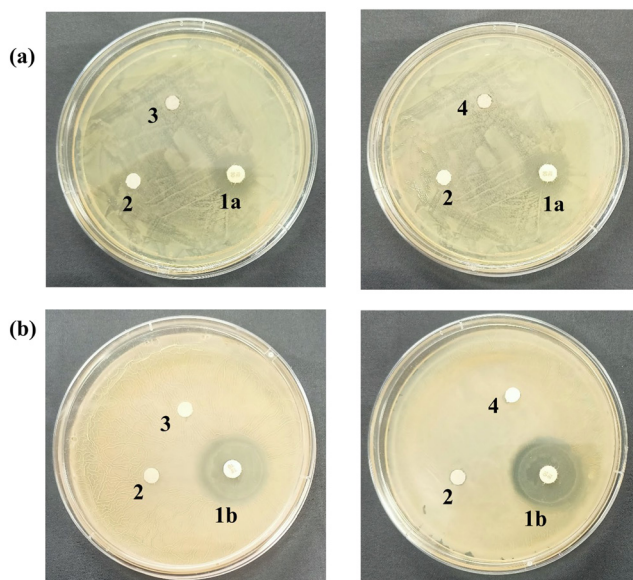

Fig. 17 *In vitro* antibacterial assay of AlGC and FeGC against (a) *E. coli* and (b) *B. subtilis*. 1a and 1b: tetracycline (positive control); 2: sterile distilled water (negative control); 3: AlGC; and 4; FeGC.

3.9.2. Development of structures. The 2D GO structure (Compound CID: 124202900) was downloaded from the PubChem database. The 2D structure was converted into 3D using Open Babel (version 2.4.0). The obtained 3D coordinates were visualized and optimized using the Avogadro software (version 1.2.0n).

The Al-MOF structure was directly retrieved from the Cambridge Crystallographic Data Centre (CCDC) with the identifier CCDC: 220475. However, for the Fe-MOF structure, it was not available in the CCDC database. Therefore, a Cr-MOF structure (CCDC: 605510) was used as a basis, and Cr atoms in the structure were replaced with Fe atoms to create the Fe-MOF model structure.

The MOF–GO composite structure was developed by combining the GO structure with the MOF structure using VESTA and Marvin (Fig. 18).[82] Subsequently, the composite structures were refined using UCSF Chimera for optimization and improvement.[55]
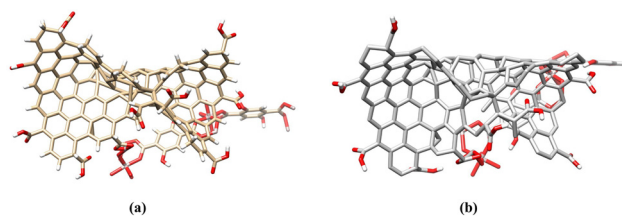

Fig. 18 Structures of (a) AlG and (b) FeG.

This journal is © The Royal Society of Chemistry 2024

Environ. Sci.: Water Res. Technol., 2024, **10**, 1938–1963 | 1957

Table 9 Binding energies and residues of certain protein targets that interact with AlGC and FeGC

Protein targets	Ligands	Binding energy (kcal mol^{-1})	Interacting residues
Bacillus subtilis-FtsZ	AlG	−2.85	SER152, ASP167, GLU251
	FeG	−2.66	ARG168, ALA252
Escherichia coli-GyraseB	AlG	−2.15	TYR26, VAL118
	FeG	−2.75	MET25, TYR26, GLY119

3.9.3. *In silico* studies. Molecular docking studies were performed to evaluate the composites' molecular interaction pattern and binding energy (AlG and FeG) with the selected microorganisms *Bacillus subtilis* and *Escherichia coli*.

AlG displayed a binding energy of −2.85 kcal mol^{-1} for the protein target of *Bacillus subtilis*–FtsZ. Table 9 displays the bonded and non-bonded interactions between residues in the active site region and the composites.

The hydrogen bonds (H-bonds) were formed between AlG and the active site regions of the protein target along with the residues of SER152, ASP167, and GLU251 with a bond length (donor–acceptor distance) of 2.87, 3.19, and 2.98 Å, respectively [Fig. 19a(i)]. Similarly, FeG exhibited a binding energy of −2.66 kcal mol^{-1}, with observed H-bond interactions with ARG168 and ALA252 residues with a bond length of 2.77 and 2.98 Å, respectively, and possessed a binding energy of −2.66 kcal mol^{-1} [Fig. 19a(ii)]. The composite framework exhibited the least binding affinity with the tested protein target of *Bacillus subtilis*–FtsZ.

Similarly, in the context of the GyraseB protein target of *Escherichia coli*, the AlG model structure established an interaction with a binding energy of −2.15 kcal mol^{-1} (Table 9). The interaction involved forming H-bonds with

TYR26 and VAL118 residues of the targeted protein, with bond lengths of 2.93 and 3.2 Å, respectively [Fig. 19b(i)]. On the other hand, FeG engaged with the MET25, TYR26, and GLY119 residues by forming H-bonds, with estimated bond lengths of 2.8, 3.34, and 3.5 Å, and exhibited a binding energy of −2.75 kcal mol^{-1} [Fig. 19b(ii)]. The atoms in the framework of AlG and FeG achieved fewer substantial interactions with the GyraseB protein target.

Overall, the comprehensive studies on antimicrobial activity and molecular docking analysis have unequivocally demonstrated that the tested composites (AlG and FeG) exerted no detrimental effect on the targeted microorganisms, *i.e.*, *Bacillus subtilis* and *Escherichia coli*. Moreover, the interactions between these compounds and the protein target were found to be relatively weak, indicating a limited affinity. These findings emphasize that the developed composites have no detrimental effects on the soil-beneficial organisms, suggesting the environmental friendliness of the developed composites.

3.10. Comparison with other adsorbents

Table 10 compares the maximum adsorption capacity of the developed MOF–GO composites for MO and MB dyes and the status of an ecotoxicity analysis against other reported adsorbents in the literature. The results demonstrated significantly higher dye adsorption values of 577 ± 37 and 631 ± 42 mg g^{-1} for MO and 336 ± 13 and 387 ± 7 mg g^{-1} for MB using the composites AlGC and FeGC, respectively, compared to the previously reported MOF-based adsorbents. This enhancement can be attributed to surface functionalization with phytochemical extract. To the best of our knowledge, the present study evaluated for the first time the eco-friendliness of MOF-based composites by antimicrobial activity as well as molecular docking-based ecotoxicity assessment.

3.11. Cost analysis

The material costs are crucial for determining the financial implications of large-scale industrial operations. Table 11 provides the details of material costs to synthesize AlGC and FeGC composites. The cost of synthesizing 1 g of AlGC and FeGC from industrial-grade chemicals has been estimated to be INR 32.84 (0.39 USD) and INR 12.5 (0.15 USD), respectively. Interestingly, based on the maximum dye sorption capacity, the estimated cost of AlGC and FeGC to remove 1 g of dye has been estimated as INR 56.8 (0.68 USD) & INR 51.88 (0.62 USD)
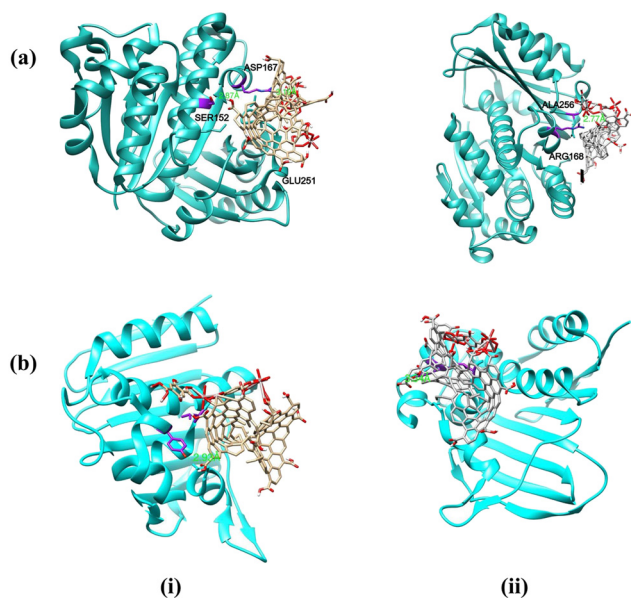
Fig. 19 Molecular docking and visualization of (a) *Bacillus subtilis*-FtsZ, and (b) *Escherichia coli*-GyraseB with (i) AlG and (ii) FeG structure models.

Table 10 Comparative maximum sorption capacity of synthesized composites with other reported MOFs

Adsorbent	Dye(s)	Q_{max} (mg g^{-1})	Toxicity status	Ref.
Fe$_3$O$_4$@MIL-101@PPI	MO	109	NA	32
	MB	219		
UiO-66-NO$_2$	MO	142.9	NA	83
	MB	41.7		
MoS$_2$–COOH@UiO-66-NH$_2$	MO	16.7	NA	33
	MB	253		
Co(ii)-MOF	MO	52.27	NA	84
	MB	64.13		
Fe$_3$O$_4$@UiO-66	MO	244	NA	34
	MB	205		
ZIF-67 composite	MO	180.50	NA	85
	MB	57.24		
Fe@Ni-MOF–2COOH	MO	225.15	NA	86
	MB	45.35		
Fe@Cu-MOF–2COOH	MO	20.32	NA	86
	MB	45.35		
Polyoxometalate/CoFe$_2$O$_4$/MIL-101(Cr)	MB	200	NA	87
AlGC	MO	577 ± 37	Ecofriendly	Present study
	MB	336 ± 13		
FeGC	MO	631 ± 42	Ecofriendly	Present study
	MB	387 ± 7		

for MO, and INR 37.12 (0.44 USD) & INR 32.25 (0.39 USD) for MB, respectively. This cost is found to be the lowest in comparison to the other MOF-based sorbent materials commonly used in wastewater treatment.[88] This lowest cost

Table 11 Cost estimation for preparing 1 g of AlGC and FeGC composites

S. No.	Components	Quantity required to make 1.0 g of AlGC	Quantity required to make 1.0 g of FeGC	Unit cost (industrial grade)/g or mL (INR)	Make	Actual cost AlGC/FeGC (INR)	Total cost for making AlGC/FeGC (INR)
1	TPA	1.37 g	0.75 g	—	—	—	32.84/12.5
2	PET bottles	6.87 g	3.76 g	—	—	—	
3	NaOH	3.44 g	1.88 g	0.019	A B Enterprises, India	0.065/0.035	
4	DMF	97.5 mL	69.7 mL	0.175	Gayatri Industries, India	17/12	
5	HCl	0.119 mL	0.68 mL	0.005	Alpha Chemika, India	0.0005/0.003	
6	Al(NO$_3$)$_3$·9H$_2$O	2.09 g	—	—	—	—	
7	Aluminum foil	6.98 g	—	—	—	—	
8	HCl	69.7 mL	—	0.005	Alpha Chemika, India	0.34/–	
9	HNO$_3$	139.4 mL	—	0.109	Golden Trading Co., India	15/–	
10	FeCl$_3$·6H$_2$O	—	2.45 g	0.034	Sudharshan Chem	–/0.008	
11	GO	0.104 g	0.123 g	—	—	—	
12	HCl	4.93 mL	4.93 mL	0.005	Alpha Chemika, India	0.02/0.02	
13	Graphite	0.069 g	0.082 g	0.08	Ecosense Labs India Pvt. Ltd., India	0.005/0.006	
14	H$_2$SO$_4$	1.36 mL	1.75 mL	0.01	Surya Fine Chem, India	0.01/0.01	
15	NaNO$_3$	0.034 g	0.04 g	0.053	Vrushabh Enterprise, India	0.001/0.002	
16	H$_3$PO$_4$	0.153 mL	0.17 mL	0.12	Meru Chem Pvt. Ltd., India	0.018/0.02	
17	KMnO$_4$	0.209 g	0.244 g	0.295	Sai Chemicals, India	0.06/0.07	
18	H$_2$O$_2$ (30% w/v)	0.17 mL	0.17 mL	1.98	ARK Chemicals, India	0.33/0.33	

could be attributed to the possibility of using waste resources as raw materials for the synthesis of AlGC and FeGC and their higher dye adsorption capacity. Moreover, FeGC emerges as a highly effective low-cost adsorbent compared to AlGC, indicating the potential low-cost adsorbent option for removing dyes (MO & MB) from industrial effluent.

4. Conclusions

In conclusion, *Moringa oleifera* leaves powder extract functionalized composites exhibited maximum adsorption capacity for MO (AlGC: 580 ± 9.8 and FeGC: 470 ± 9.7 mg g^{-1}) and MB (AlGC: 320 ± 10.9 and FeGC: 350 ± 11.28 mg g^{-1}) dyes in comparison to the other tested adsorbents. Composite mass and initial dye concentration were established as significant factors for the maximum adsorption of dyes by Taguchi optimization. The optimal conditions for maximizing the removal of MO dye using AlGC and FeGC composites were achieved at 30 min, 10 mg dosage, and 30 °C through Taguchi optimization. Similarly, for MB dye, the optimal parameters were 120 min, 10 mg dosage, and 30 °C. The maximum dye adsorption capacity under optimum conditions was obtained as 483.29 & 477.67 mg g^{-1} for MO and 294.08 and 291.84 mg g^{-1} for MB with AlGC and FeGC composites, respectively. The significant presence of –OH, C=O, and –COOH functional groups on functionalized composite surfaces acted as active sites for the enhanced MO and MB adsorption due to the electrostatic attraction (here, incorporate conclusion based on BET, TGA and XPS analysis before and after adsorption). Kinetic, isotherm, and thermodynamic modeling results suggested that the MO and MB adsorption on the composite surface was a physical, spontaneous, and exothermic process. The Langmuir isotherm model confirmed monolayer coverage of MO and MB over the surface of the composite. The synthesized composites showed more than ~65% dye removal efficiency after three adsorption–desorption cycles, which indicates their applicability at large-scale operations. The antimicrobial activity and molecular docking analysis confirmed the non-toxicity of composites as they demonstrated very low affinity towards the targeted microorganisms, *i.e.*, *Bacillus subtilis* and *Escherichia coli*, which indicates their safe use and disposal in a natural soil environment. The cost study established that FeGC outperforms AlGC as a highly efficient low-cost adsorbent, suggesting a possible low-cost adsorbent choice for the removal of dyes (MO & MB) from industrial wastewater.

Abbreviations

q_{exp}	Achieved/experimental adsorption capacity
Q_m	Adsorption Affinity
K_F	Adsorption capacity
q	Adsorption capacity
$1/n$	Adsorption intensity
E	Adsorption intensity
α	Adsorption rate
AlGC	Al-MOF/GO composite
Al-MOF	Aluminium terephthalate MOF
Al	Aluminum
Al^{3+}	Aluminum ion with +3 oxidation state
$Al(NO_3)_3$	Aluminum nitrate
$Al(NO_3)_3 \cdot 9H_2O$	Aluminum nitrate nonahydrate
NH_2–TPA	Amino–terephthalic acid
AR	Analytical grade
~	Approximation
BJH	Barrett–Joyner–Halenda
BET	Brunauer–Emmett–Teller
CCDC	Cambridge Crystallographic Data Centre
C	Carbon
C–H	Carbon–hydrogen bond
C=O	Carboxyl group
–COOH	Carboxylic acid
R^2	Coefficient of determination
CFU	Colony forming unit
C	Concentration
β	Desorption rate
dia	Diameter
K_d	Distribution coefficient
D–R	Dubinin–Radushkevich
EDS	Energy dispersive spectroscopy
K_C	Equilibrium constant
EG	Ethylene glycol
FeG	Fe-MOF/GO composite
FESEM	Field emission scanning electron microscope
C_f	Final concentration
F-test	Fisher's test
FTIR	Fourier-transform infrared spectroscopy
AlGC	Functionalized Al-MOF/GO composite
FeGC	Functionalized Fe-MOF/GO composite
g	Grams
GO	Graphene oxide
B	Heat of adsorption
h	Hours
HCl	Hydrochloric acid
H_2O_2	Hydrogen peroxide
–OH	Hydroxyl groups
C_0	Initial concentration
Fe	Iron
$FeCl_3 \cdot 6H_2O$	Iron chloride hexahydrate
Fe^{3+}	Iron ion with +3 oxidation state
Fe-MOF	Iron terephthalate MOF
Fe–O	Iron–oxygen bond interaction
K	Kelvin
MOF	Metal organic framework
MO	Methyl orange
MB	Methylene blue
mcg/disc	Micrograms per disc
μL	Microlitre
mL	Milliliters
mg	Milligram
min	Minutes

1960 | *Environ. Sci.: Water Res. Technol.*, 2024, **10**, 1938–1963

This journal is © The Royal Society of Chemistry 2024

M	Molarity
MP	*Moringa* powder
DMF	*N,N*-Dimethyl formamide
HNO_3	Nitric acid
No.	Number
n	Number of tests
OFAT	One factor at a time
η_{opt}	Optimized S/N ratio's total mean
O	Oxygen
pH_{ZPC}	pH at zero-point charge
H_3PO_4	Phosphoric acid
PET	Polyethylene terephthalate
pH	Potential of hydrogen
q_{pred}	Predicted adsorption capacity
R_{opt}	Predicted response
k_1 and k_2	Rate constants
P/P_0	Ratio of absolute pressure to the saturation vapor pressure
RPM	Rotations per minute
$(\bar{\eta}_i)$	S/N ratio's mean at the optimum level
η_m	S/N ratio's total mean
SEM	Scanning electron microscopy
R_L	Separation constant
S/N	Signal-to-noise
NaOH	Sodium hydroxide
ΔH°	Standard enthalpy
ΔS°	Standard entropy
ΔG°	Standard Gibbs free energy
TPA	Terephthalic acid
y_i	The individual's adsorption capacity at the 'ith' experiment
MTCC	The Microbial Type Culture Collection and Gene Bank
3D	Three dimension
2D	Two dimension
UV-vis	Ultraviolet visible spectroscopy
v/v	Volume/volume
wt%	Weight percentage
XRD	X-ray diffraction

Author contributions

Anil Kumar K.: conceptualization, methodology, experimentation, investigation, data curation, writing – original document, formal analysis, reviewing, and editing. Arpit Bisoi: experimentation, data curation. Yeshwanth M.: molecular docking studies, writing. Shobham: antibacterial studies, writing. Mohan Jujaru: reviewing and editing. Jitendra Panwar: conceptualization, supervision, reviewing, and editing. Suresh Gupta: conceptualization, supervision, reviewing, and editing.

Conflicts of interest

There are no conflicts to declare.

Acknowledgements

References

1 E. R. Jones, M. T. H. van Vliet, M. Qadir and M. F. P. Bierkens, *Earth Syst. Sci. Data*, 2021, **13**, 237–254.

2 M. Bilal, J. Ali, K. Bibi, S. B. Khan, M. Saqib, R. Saeed, R. Javeria, H. Khan, K. Akhtar and E. M. Bakhsh, *Ind. Crops Prod.*, 2022, **187**, 115267.

3 R. R. Karri, M. Tanzifi, M. Tavakkoli Yaraki and J. N. Sahu, *J. Environ. Manage.*, 2018, **223**, 517–529.

4 U. Maheshwari and S. Gupta, *Process Saf. Environ. Prot.*, 2016, **102**, 547–557.

5 L. Mouni, L. Belkhiri, J.-C. Bollinger, A. Bouzaza, A. Assadi, A. Tirri, F. Dahmoune, K. Madani and H. Remini, *Appl. Clay Sci.*, 2018, **153**, 38–45.

6 M. Yadav, R. Gupta and R. K. Sharma, in *Advances in Water Purification Techniques*, Elsevier, 2019, pp. 355–383.

7 R. Bouchareb, K. Derbal, Y. Özay, Z. Bilici and N. Dizge, *J. Water Process Eng.*, 2020, **37**, 101521.

8 J. Wu, J. Wang, Y. Du, H. Li and X. Jia, *J. Nanopart. Res.*, 2016, **18**, 191.

9 M. M. Sabzehmeidani, S. Mahnaee, M. Ghaedi, H. Heidari and V. A. L. Roy, *Mater. Adv.*, 2021, **2**, 598–627.

10 J. Shu, S. Cheng, H. Xia, L. Zhang, J. Peng, C. Li and S. Zhang, *RSC Adv.*, 2017, **7**, 14395–14405.

11 S. E. Lakroun, K. Boutemak, A. Haddad, E. M. Bouchareb and R. Bouchareb, *Energy Sources, Part A*, 2023, **45**, 3138–3153.

12 H.-C. "Joe" Zhou and S. Kitagawa, *Chem. Soc. Rev.*, 2014, **43**, 5415–5418.

13 A. D. Pournara, A. Margariti, G. D. Tarlas, A. Kourtelaris, V. Petkov, C. Kokkinos, A. Economou, G. S. Papaefstathiou and M. J. Manos, *J. Mater. Chem. A*, 2019, **7**, 15432–15443.

14 R. Ettlinger, U. Lächelt, R. Gref, P. Horcajada, T. Lammers, C. Serre, P. Couvreur, R. E. Morris and S. Wuttke, *Chem. Soc. Rev.*, 2022, **51**, 464–484.

15 J. Zolgharnein and S. Dermanaki Farahani, *J. Chemom.*, 2023, **37**, 6–8.

16 A. Aguado, L. Martínez, L. Becerra, M. Arieta-araunabeña, S. Arnaiz, A. Asueta and I. Robertson, *J. Mater. Cycles Waste Manage.*, 2014, **16**, 201–210.

17 W. Yang, R. Liu, C. Li, Y. Song and C. Hu, *Waste Manage.*, 2021, **135**, 267–274.

18 M. Lu, L. Li, S. Shen, D. Chen and W. Han, *New J. Chem.*, 2019, **43**, 1032–1037.

19 T. Chowdhury, L. Zhang, J. Zhang and S. Aggarwal, *Mater. Adv.*, 2021, **2**, 3051–3059.

20 G. K. Ramesha, A. Vijaya Kumara, H. B. Muralidhara and S. Sampath, *J. Colloid Interface Sci.*, 2011, **361**, 270–277.

21 U. Ciesla, D. Demuth, R. Leon, P. Petroff, G. Stucky, K. Unger and F. Schüth, *J. Chem. Soc., Chem. Commun.*, 1994, 1387–1388.

This journal is © The Royal Society of Chemistry 2024

Environ. Sci.: Water Res. Technol., 2024, **10**, 1938–1963 | **1961**

22 H. Itoh and T. Sugimoto, *J. Colloid Interface Sci.*, 2003, **265**, 283–295.

23 A. B. Chin and I. I. Yaacob, *J. Mater. Process. Technol.*, 2007, **191**, 235–237.

24 Y. Abdallah, S. O. Ogunyemi, A. Abdelazez, M. Zhang, X. Hong, E. Ibrahim, A. Hossain, H. Fouad, B. Li and J. Chen, *BioMed Res. Int.*, 2019, **2019**, 1–8.

25 B. K. Sharma, B. R. Mehta, V. P. Chaudhari, E. V. Shah, S. Mondal Roy and D. R. Roy, *J. Cluster Sci.*, 2022, **33**, 1667–1675.

26 R. Bouchareb, K. Derbal and A. Benalia, *Water Sci. Technol.*, 2021, **84**, 393–403.

27 R. Bouchareb, K. Derbal, A. Yelfouf, D. Ben Diaf, E. Mahfouf Bouchareb and N. Dizge, *Clean: Soil, Air, Water*, 2021, **49**, 1–7.

28 A. Kumar, K. Shobham, J. Panwar and S. Gupta, *Environ. Sci. Pollut. Res.*, 2022, **30**, 61541–61561.

29 B. R. Patra, S. Nanda, A. K. Dalai and V. Meda, *Chemosphere*, 2021, **285**, 131531.

30 M. Nalbant, H. Gökkaya and G. Sur, *Mater. Des.*, 2007, **28**, 1379–1385.

31 A. S. Yusuff, O. A. Ajayi and L. T. Popoola, *Sci. Afr.*, 2021, **13**, e00850.

32 H. S. Far, M. Hasanzadeh, M. Najafi and M. Rabbani, *J. Inorg. Organomet. Polym. Mater.*, 2022, **32**, 3848–3863.

33 K. Karami, P. Bayat, S. Javadian and M. Saraji, *J. Mol. Liq.*, 2021, **342**, 117520.

34 S. Ahmadipouya, M. Heidarian Haris, F. Ahmadijokani, A. Jarahiyan, H. Molavi, F. Matloubi Moghaddam, M. Rezakazemi and M. Arjmand, *J. Mol. Liq.*, 2021, **322**, 114910.

35 A. Kumar, K. Y. Mahesh, J. Panwar and S. Gupta, *Environ. Sci. Pollut. Res.*, 2024, **31**, 21545–21567.

36 B. Das, R. Kundu and S. Chakravarty, *Mater. Chem. Phys.*, 2022, **290**, 126597.

37 A. Kumar, K. M. Yeshwanth, K. Kumar, B. J. Panwar and S. Gupta, *J. Environ. Manage.*, 2022, **307**, 114523.

38 S. K. Pradhan, J. Panwar and S. Gupta, *J. Environ. Chem. Eng.*, 2017, **5**, 5801–5814.

39 H. R. Mahdipoor, R. Halladj, E. Ganji Babakhani, S. Amjad-Iranagh and J. Sadeghzadeh Ahari, *RSC Adv.*, 2021, **11**, 5192–5203.

40 L.-L. Hsieh, H.-J. Kang, H.-L. Shyu and C.-Y. Chang, *Water Sci. Technol.*, 2009, **60**, 1295–1301.

41 N. Berkane, S. Meziane and S. Aziri, *Sep. Sci. Technol.*, 2020, **55**, 278–288.

42 S. Gupta and B. V. Babu, *Chem. Eng. J.*, 2009, **150**, 352–365.

43 A. Z. El-Sonbati, N. F. Omar, M. I. Abou-Dobara, M. A. Diab, M. A. El-Mogazy, S. M. Morgan, M. A. Hussien and A. A. El-Ghettany, *J. Mol. Struct.*, 2021, **1239**, 130481.

44 S. G. Nozha, S. M. Morgan, S. E. A. Ahmed, M. A. El-Mogazy, M. A. Diab, A. Z. El-Sonbati and M. I. Abou-Dobara, *J. Mol. Struct.*, 2021, **1227**, 129525.

45 CLSI, *Methods for Dilution Antimicrobial Susceptibility Tests for Bacteria That Grow Aerobically; Approved Standard —*

Ninth Edition, CLSI document M07-A9, Wayne, Clinical and Laboratory Standard Institute, 2012, vol. 32.

46 A. W. Bauer, *Arch. Intern. Med.*, 1959, **104**, 208.

47 N. Jain, P. Alam, I. R. Laskar and J. Panwar, *RSC Adv.*, 2015, **5**, 61983–61988.

48 S. K. Pradhan, V. Pareek, J. Panwar and S. Gupta, *J. Water Process Eng.*, 2019, **32**, 100917.

49 A. Allouche, *J. Comput. Chem.*, 2012, **32**, 174–182.

50 S. Prasad, L. C. Malav, J. Choudhary, S. Kannojiya, M. Kundu, S. Kumar and A. N. Yadav, *Current Trends in Microbial Biotechnology for Sustainable Agriculture*, Springer, 2021, pp. 1–21.

51 A. Ortiz and E. Sansinenea, *Sustainability*, 2022, **14**, 5358.

52 M. A. Oliva, D. Trambaiolo and J. Löwe, *J. Mol. Biol.*, 2007, **373**, 1229–1242.

53 S. Narramore, C. E. M. Stevenson, A. Maxwell, D. M. Lawson and C. W. G. Fishwick, *Bioorg. Med. Chem.*, 2019, **27**, 3546–3550.

54 N. Guex and M. C. Peitsch, *Electrophoresis*, 1997, **18**, 2714–2723.

55 E. F. Pettersen, T. D. Goddard, C. C. Huang, G. S. Couch, D. M. Greenblatt, E. C. Meng and T. E. Ferrin, *J. Comput. Chem.*, 2004, **25**, 1605–1612.

56 W. L. DeLano, *{CCP4} Newsletter On Protein Crystallography*, 2002, vol. 40, pp. 1–8.

57 K. Zhu, Y. Liu and J. Liu, *RSC Adv.*, 2014, **4**, 42278–42284.

58 F. Ahmadijokani, S. Ahmadipouya, H. Molavi and M. Arjmand, *Dalton Trans.*, 2019, **48**, 13555–13566.

59 Z. Liu, W. He, Q. Zhang, H. Shapour and M. F. Bakhtari, *ACS Omega*, 2021, **6**, 4597–4608.

60 M. Majumder, R. B. Choudhary, A. K. Thakur, A. Khodayari, M. Amiri, R. Boukherroub and S. Szunerits, *Electrochim. Acta*, 2020, **353**, 136609.

61 J. M. Moreno, A. Velty, U. Díaz and A. Corma, *Chem. Sci.*, 2019, **10**, 2053–2066.

62 Q. Xie, Y. Li, Z. Lv, H. Zhou, X. Yang, J. Chen and H. Guo, *Sci. Rep.*, 2017, **7**, 3316.

63 J. Rouquerol, D. Avnir, C. W. Fairbridge, D. H. Everett, J. M. Haynes, N. Pernicone, J. D. F. Ramsay, K. S. W. Sing and K. K. Unger, *Pure Appl. Chem.*, 1994, **66**, 1739–1758.

64 L. Xu, J. Zhang, J. Ding, T. Liu, G. Shi, X. Li, W. Dang, Y. Cheng and R. Guo, *Minerals*, 2020, **10**, 72.

65 S. Luo and J. Wang, *Environ. Sci. Pollut. Res.*, 2018, **25**, 5521–5528.

66 B. Boukoussa, A. Hakiki, S. Moulai, K. Chikh, D. E. Kherroub, L. Bouhadjar, D. Guedal, K. Messaoudi, F. Mokhtar and R. Hamacha, *J. Mater. Sci.*, 2018, **53**, 7372–7386.

67 P. Praipipat, P. Ngamsurach and K. Pratumkaew, *Arabian J. Chem.*, 2023, **16**, 104640.

68 R. Chikri, N. Elhadiri, M. Benchanaa and Y. El Maguana, *J. Chem.*, 2020, **2020**(1), 8813420.

69 N. Unlu and M. Ersoz, *J. Hazard. Mater.*, 2006, **136**, 272–280.

70 A. Elaziouti and N. Laouedj, *J. Korean Chem. Soc.*, 2011, **55**, 208–217.

1962 | *Environ. Sci.: Water Res. Technol.*, 2024, **10**, 1938–1963

This journal is © The Royal Society of Chemistry 2024

71 T. Shahzadi, S. Sanaullah, T. Riaz, M. Zaib, A. Kanwal and H. Jabeen, *Environ. Dev. Sustain.*, 2021, **23**, 17923–17941.

72 P. Senthil Kumar, P. S. A. Fernando, R. T. Ahmed, R. Srinath, M. Priyadharshini, A. M. Vignesh and A. Thanjiappan, *Chem. Eng. Commun.*, 2014, **201**, 1526–1547.

73 A. Pourjavadi, M. Nazari, M. Kohestanian and S. H. Hosseini, *Colloid Polym. Sci.*, 2019, **297**, 917–926.

74 A. Wathukarage, I. Herath, M. C. M. Iqbal and M. Vithanage, *Environ. Geochem. Health*, 2019, **41**, 1647–1661.

75 M. Shahnawaz Khan, M. Khalid and M. Shahid, *Mater. Adv.*, 2020, **1**, 1575–1601.

76 L. Yu, Z. Luo, Y. Zhang, S. Wu, C. Yang and J. Cheng, *Environ. Sci. Pollut. Res.*, 2019, **26**, 3685–3696.

77 T. Ainane, F. Khammour, M. Talbi and M. Elkouali, *Orient. J. Chem.*, 2014, **30**, 1183–1189.

78 N. N. Bahrudin, M. A. Nawi, A. H. Jawad and S. Sabar, *J. Polym. Environ.*, 2020, **28**, 1901–1913.

79 J. M. Pérez-Morales, G. Sánchez-Galván and E. J. Olguín, *Environ. Sci. Pollut. Res.*, 2019, **26**, 5955–5970.

80 X. Zhao, S. Liu, Z. Tang, H. Niu, Y. Cai, W. Meng, F. Wu and J. P. Giesy, *Sci. Rep.*, 2015, **5**, 11849.

81 A. G. Femi-Adepoju, A. O. Dada, K. O. Otun, A. O. Adepoju and O. P. Fatoba, *Heliyon*, 2019, **5**, e01543.

82 K. Momma and F. Izumi, *J. Appl. Crystallogr.*, 2011, **44**, 1272–1276.

83 H. T. Dinh, N. T. Tran and D. X. Trinh, *J. Anal. Methods Chem.*, 2021, **2021**, 1–10.

84 H. A. M. Saleh, I. Mantasha, K. M. A. Qasem, M. Shahid, M. N. Akhtar, M. A. AlDamen and M. Ahmad, *Inorg. Chim. Acta*, 2020, **512**, 119900.

85 M. A. Nazir, N. A. Khan, C. Cheng, S. S. A. Shah, T. Najam, M. Arshad, A. Sharif, S. Akhtar and A. ur Rehman, *Appl. Clay Sci.*, 2020, **190**, 105564.

86 M. N. Ahamad, M. S. Khan, M. Shahid and M. Ahmad, *Dalton Trans.*, 2020, **49**, 14690–14705.

87 A. Jarrah and S. Farhadi, *RSC Adv.*, 2020, **10**, 39881–39893.

88 L. Biswal, J. E. Goodwill, C. Janiak and S. Chatterjee, *Sep. Purif. Rev.*, 2022, **51**, 408–426.

This journal is © The Royal Society of Chemistry 2024

Environ. Sci.: Water Res. Technol., 2024, **10**, 1938–1963 | **1963**